Article

Developmental Cell

Opposing Effects of *CREBBP* Mutations Govern the Phenotype of Rubinstein-Taybi Syndrome and Adult SHH Medulloblastoma

Graphical Abstract

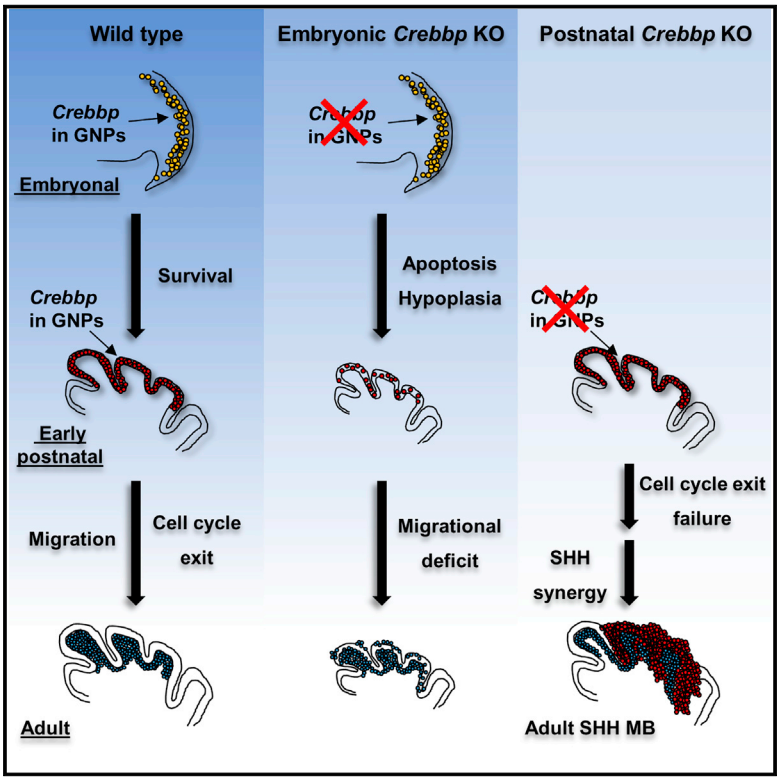

Highlights

- *CREBBP* mutations in human medulloblastoma deplete acetyltransferase activity
- *Crebbp* mutations exert opposing effects during cerebellar development
- Embryonal loss of *Crebbp* impairs normal cerebellar development
- Postnatal loss of *Crebbp* synergizes with Shh to drive growth of medulloblastoma

Authors

Daniel J. Merk, Jasmin Ohli, Natalie D. Merk, ..., Lukas Chavez, Marcel Kool, Ulrich Schüller

Correspondence

u.schueller@uke.de

In Brief

Merk et al. show that the developmental time frame of *CREBBP* mutation acquisition in cerebellar granule neurons determines the pathogenic effect of these alterations in the cerebellum. These time-sensitive consequences explain phenotypic differences seen in patients with germline (Rubinstein-Taybi syndrome) or somatic mutations (adult SHH medulloblastoma) of *CREBBP*.

Merk et al., 2018, Developmental Cell *44*, 709–724
March 26, 2018
https://doi.org/10.1016/j.devcel.2018.02.012

CellPress

Developmental Cell
Article

Opposing Effects of *CREBBP* Mutations Govern the Phenotype of Rubinstein-Taybi Syndrome and Adult SHH Medulloblastoma

Daniel J. Merk,[1,2,3] Jasmin Ohli,[1] Natalie D. Merk,[4] Venu Thatikonda,[5] Sorana Morrissy,[6,7] Melanie Schoof,[8] Susanne N. Schmid,[1,9] Luke Harrison,[1] Severin Filser,[10] Julia Ahlfeld,[1,11] Serap Erkek,[5,12,13] Kaamini Raithatha,[14] Thomas Andreska,[15] Marc Weißhaar,[1] Michael Launspach,[1] Julia E. Neumann,[1,16] Mehdi Shakarami,[17] Dennis Plenker,[18] Marco A. Marra,[19,20] Yisu Li,[19] Andrew J. Mungall,[19] Richard A. Moore,[19] Yussanne Ma,[19] Steven J.M. Jones,[19]

(Author list continued on next page)

[1]Center for Neuropathology, Ludwig-Maximilians-University, 81377 Munich, Germany
[2]Cancer Biology and Pediatric Oncology, Dana-Farber Cancer Institute, Boston, MA 02215, USA
[3]Neurobiology, Harvard Medical School, Boston, MA 02215, USA
[4]Munich Center for Integrated Protein Science at the Chemistry Department, Technical University, 85747 Munich, Germany
[5]Division of Pediatric Neurooncology, German Cancer Research Center (DKFZ), 69120 Heidelberg, Germany
[6]Arthur and Sonia Labatt Brain Tumour Research Centre and Division of Neurosurgery, Hospital for Sick Children (HSC), Toronto, ON M5G 1L7, Canada
[7]Program in Developmental and Stem Cell Biology, HSC, Toronto, ON M5G 1X8, Canada
[8]Research Institute Children's Cancer Center Hamburg, Martinistrasse 52, N63 (HPI), Hamburg 20251, Germany
[9]Department of Neuropathology, University Medical Center Göttingen, 37099 Göttingen, Germany
[10]German Center for Neurodegenerative Diseases (DZNE), Ludwig-Maximilians-University, 81377 Munich, Germany
[11]Division of Clinical Pharmacology, Department of Internal Medicine IV, Ludwig-Maximilians-University, 80337 Munich, Germany
[12]European Molecular Biology Laboratory (EMBL), Genome Biology Unit, 69117 Heidelberg, Germany
[13]German Cancer Consortium (DKTK), Core Center Heidelberg, 69120 Heidelberg, Germany
[14]Microarray and Deep-Sequencing Core Facility, University Medical Center Göttingen, 37077 Göttingen, Germany
[15]Institute for Clinical Neurobiology, University of Würzburg, 97078 Würzburg, Germany
[16]Institute of Neuropathology, University Medical Center, Hamburg-Eppendorf, 20246 Hamburg, Germany
[17]Walter Brendel Center of Experimental Medicine, Ludwig-Maximilians-University, 81377 Munich, Germany
[18]Department of Translational Genomics, University of Cologne, 50931 Cologne, Germany
[19]Canada's Michael Smith Genome Sciences Centre, BC Cancer Agency, Vancouver, BC VSZ 4S6, Canada
[20]Department of Medical Genetics, University of British Columbia, Vancouver, BC V6H 3N1, Canada
[21]Institute of Physiological Chemistry, University Medical Center of the Johannes Gutenberg University, 55128 Mainz, Germany
[22]Institute of Clinical Radiology, Ludwig-Maximilians-University, 81377 Munich, Germany
[23]Department of Pediatric Neuroradiology, Istituto Giannina Gaslini, 16147 Genova, Italy
[24]Institute of Human Genetics, Christian-Albrechts-University and University Hospital Schleswig-Holstein, Campus Kiel, 24105 Kiel, Germany

(Affiliations continued on next page)

SUMMARY

Recurrent mutations in chromatin modifiers are specifically prevalent in adolescent or adult patients with Sonic hedgehog-associated medulloblastoma (SHH MB). Here, we report that mutations in the acetyltransferase *CREBBP* have opposing effects during the development of the cerebellum, the primary site of origin of SHH MB. Our data reveal that loss of *Crebbp* in cerebellar granule neuron progenitors (GNPs) during embryonic development of mice compromises GNP development, in part by downregulation of brain-derived neurotrophic factor (*Bdnf*). Interestingly, concomitant cerebellar hypoplasia was also observed in patients with Rubinstein-Taybi syndrome, a congenital disorder caused by germline mutations of *CREBBP*. By contrast, loss of *Crebbp* in GNPs during postnatal development synergizes with oncogenic activation of SHH signaling to drive MB growth, thereby explaining the enrichment of somatic *CREBBP* mutations in SHH MB of adult patients. Together, our data provide insights into time-sensitive consequences of *CREBBP* mutations and corresponding associations with human diseases.

INTRODUCTION

Medulloblastoma (MB) is an aggressively growing tumor of neuroectodermal origin that arises in the posterior fossa. Survival rates have significantly increased in the last decades, but still approximately one-third of the patients succumb to their disease. Moreover, survivors often suffer from severe treatment-related long-term sequelae (Smoll, 2012). Advancing technologies in

Beat Lutz,[21] Birgit Ertl-Wagner,[22] Andrea Rossi,[23] Rabea Wagener,[24,25] Reiner Siebert,[24,25] Andreas Jung,[26] Charles G. Eberhart,[27] Boleslaw Lach,[28] Michael Sendtner,[15] Stefan M. Pfister,[5,13,29] Michael D. Taylor,[6,7,30] Lukas Chavez,[5] Marcel Kool,[5,13] and Ulrich Schüller[1,8,16,31,32,*]

[25]Institute for Human Genetics, Ulm University and Ulm University Medical Center, 89081 Ulm, Germany
[26]Institute of Pathology, Ludwig-Maximilians-University, 81377 Munich, Germany
[27]Division of Neuropathology and Sidney Kimmel Comprehensive Cancer Center, Johns Hopkins University, Baltimore, MD 21287, USA
[28]Department of Pathology and Molecular Medicine, McMaster University, Hamilton, ON L8S 4L8, Canada
[29]Department of Pediatric Hematology and Oncology, University Hospital Heidelberg, 69120 Heidelberg, Germany
[30]Department of Laboratory Medicine and Pathobiology, University of Toronto, Toronto, ON M5S 1A8, Canada
[31]Department of Pediatric Hematology and Oncology, University Medical Center, Hamburg-Eppendorf, 20246 Hamburg, Germany
[32]Lead Contact
*Correspondence: u.schueller@uke.de
https://doi.org/10.1016/j.devcel.2018.02.012

molecular biology have tremendously changed our knowledge about the molecular mechanisms that form the basis of MB heterogeneity. The tumors are subcategorized into four major molecular subgroups (Sonic hedgehog [SHH], WNT, group 3, and group 4), as defined by gene expression or DNA methylation patterns (Hovestadt et al., 2013; Taylor et al., 2012). However, tumors within one single subgroup of MB may still differ substantially from each other in terms of biology and clinical parameters. For instance, SHH MBs occur in infants and in adults with distinct molecular characteristics (Kool et al., 2014).

Several sequencing studies have been performed broadening our knowledge of genetic alterations in human MBs (Northcott et al., 2017; Jones et al., 2012). These studies provide evidence that, among others, alterations affecting the epigenetic machinery play a functional role during MB development and/or progression across all four subgroups. Of note, we have shown that chromatin modifiers are particularly often mutated in the subgroup of adult SHH MBs (Kool et al., 2014). Among these genes is the transcriptional co-activator *CREBBP* (CREB-binding protein), which has been found to be almost exclusively mutated in adult SHH MBs, and has previously been associated with the development of different other tumor entities, such as lung cancer, lymphoma, or leukemia (Peifer et al., 2012; Mullighan et al., 2011; Pasqualucci et al., 2011). Germline mutations of *CREBBP* cause the Rubinstein-Taybi syndrome (RTS), a congenital developmental disorder with a predisposition for malignancies of the CNS, including MBs (Taylor et al., 2001; Miller and Rubinstein, 1995). This apparent association of *CREBBP* with the development of MB prompted us to investigate the impact of *CREBBP* mutations on cerebellar development and the formation of SHH MBs.

RESULTS

CREBBP Mutations in Human MB Deplete Acetyltransferase Activity

We and others have previously shown that *CREBBP* is recurrently mutated in human MB with a preponderance of mutations in adult patients (Figure 1A) (Northcott et al., 2017; Kool et al., 2014; Jones et al., 2012; Robinson et al., 2012), and we here add to this list of alterations present in adult SHH MBs (Figure 1B; Table S1). While looking at *CREBBP* expression pattern in annotated MB samples (Kool et al., 2014; Cho et al., 2011), we detected a certain heterogeneity in MB subgroups, but no correlation of *CREBBP* expression and survival in SHH MBs (Figures S1A–S1C). Furthermore, *CREBBP* mutated cases did not cluster together with respect to global gene expression pattern (Figure S1D).

As the majority of *CREBBP* mutations in MB are likely to affect the histone acetyltransferase (HAT) domain by either N-terminal stop-gain/frameshift mutations or alterations within the HAT domain (Figure 1B), we investigated their influence on HAT activity of CREBBP. Indeed, all amino acid substitutions in the HAT domain are classified as being damaging by computational analyses (Ng and Henikoff, 2003) Further analysis of the crystal structure of the HAT domain of the CREBBP homolog EP300 (Liu et al., 2008) showed that recurrent SHH MB-associated mutations are part of the substrate-binding loop L1 or are located within adjacent regions at the interface of substrate binding (Figure 1C). From those recurrent mutations, we further assessed the functional impact of the R1446L, Y1482C, and I1483F CREBBP mutations on HAT activity, thereby including one alteration (R1446L) that is not an integral part of the L1 loop. Indeed, all three mutations showed significantly reduced HAT activity in an *in vitro* assay (Figure 1D), supporting a role for loss of HAT activity of CREBBP in human SHH MB development. All identified *CREBBP* mutations in SHH MBs to date were shown to affect only one allele of *CREBBP*, indicating a mechanism that is potentially driven by haploinsufficiency or a dominant-negative form of CREBBP protein. To test the latter hypothesis, we stably expressed GFP as control alone or in combination with FLAG-tagged CREBBP protein with selected mutations in HEK293T cells carrying two endogenous wild-type alleles of *CREBBP* (Figure 1E). In line with our experimental setup, western blot analyses confirmed a significant increase in total CREBBP protein levels in clones expressing mutant CREBBP protein compared with control cells (Figures 1F and 1G). We then went on and quantified acetylation of histone H3 in these cells. Indeed, two out of three selected mutations of CREBBP protein decreased acetylation of histone H3 as determined by indirect immunofluorescence (Figures 1H and 1I), suggesting that mutated CREBBP protein might act as a dominant-negative effector over wild-type CREBBP. Together, these data show that *CREBBP* mutations found in human MB compromise HAT activity.

CREBBP Expression during Embryonic Development Is Essential for Normal Cerebellar Development in Mice and Man

Crebbp is strongly expressed in murine granule neuron progenitors (GNPs), a likely cellular origin for Shh MBs (Schüller et al.,

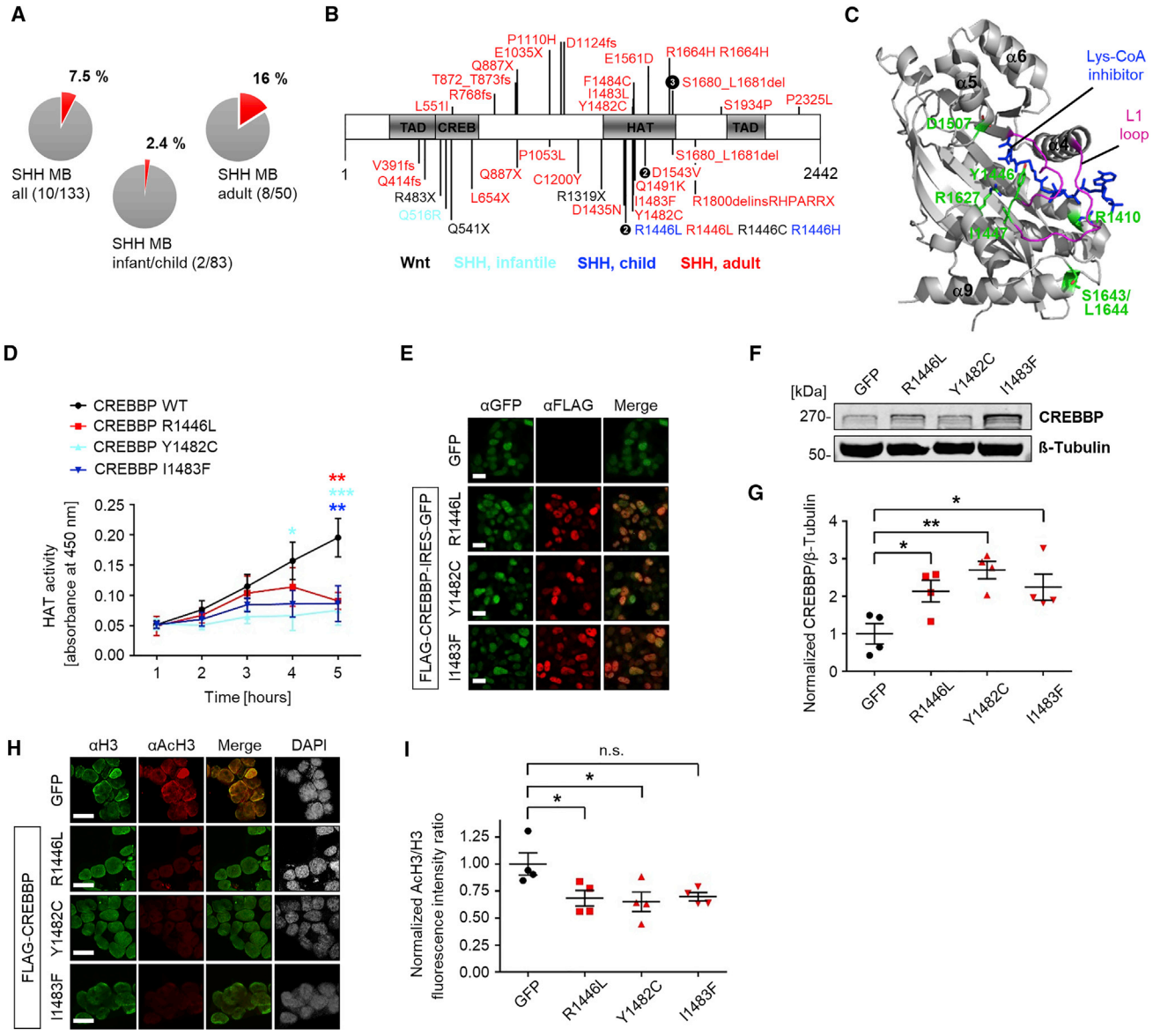

Figure 1. *CREBBP* Mutations in Human MB Deplete Acetylation Activity

(A) Incidence of *CREBBP* mutations in human SHH MB with respect to different age groups.

(B) Human CREBBP protein and selected protein domains with mutations identified in this study (above) or previously described alterations (below) in human MB. TAD, transactivation domain; CREB, CREB-binding domain; HAT, histone acetyltransferase domain. Numbers in black circles indicate the number of patients presenting this specific alteration.

(C) Amino acids in HAT domain recurrently mutated in SHH MB (R1446, Y1482, I1483, D1543, R1664, and S1680/L1681) mapped to the corresponding positions (R1410, Y1446, I1447, D1507, R1627, and S1643/L1644) in the crystal structure of the EP300 HAT domain. Lys-CoA inhibitor in blue, substrate-binding loop L1 in magenta.

(D) *In vitro* acetylation assay for human wild-type CREBBP protein and mutations R1446L, Y1482C, and I1483F (CREBBP WT: n = 4, CREBBP mutants: n = 3, Bonferroni *post-hoc* test of two-way repeated measures ANOVA).

(E) Immunofluorescence for GFP and FLAG of HEK293T cells stably expressing GFP alone or in combination with mutants of human FLAG-tagged CREBBP (R1446L, Y1482C, and I1483F). Scale bars, 15 μm.

(F) Representative western blot images for CREBBP and β-tubulin in stable HEK293T cell clones.

(G) Quantification of total CREBBP protein levels in stable HEK293T cell clones relative to β-tubulin (n = 4 monoclonal clones per construct, Bonferroni *post-hoc* test of one-way ANOVA).

(H) Immunofluorescence for total histone H3 and acetylated histone H3 (AcH3 at K9, K14, K18, K23, and K27) in HEK293T cell clones stably expressing either GFP or CREBBP R1446L, Y1482C, and I1483F mutants. Scale bars, 15 μm.

(I) Quantification of chromatin acetylation using indirect immunofluorescence from AcH3 relative to total histone H3 per nucleus (n = 4 monoclonal clones per construct, Bonferroni *post-hoc* test of one-way ANOVA).

All graphs display mean ± SEM. *p ≤ 0.05, **p ≤ 0.01, ***p ≤ 0.001, n.s., not significant. See also Figure S1.

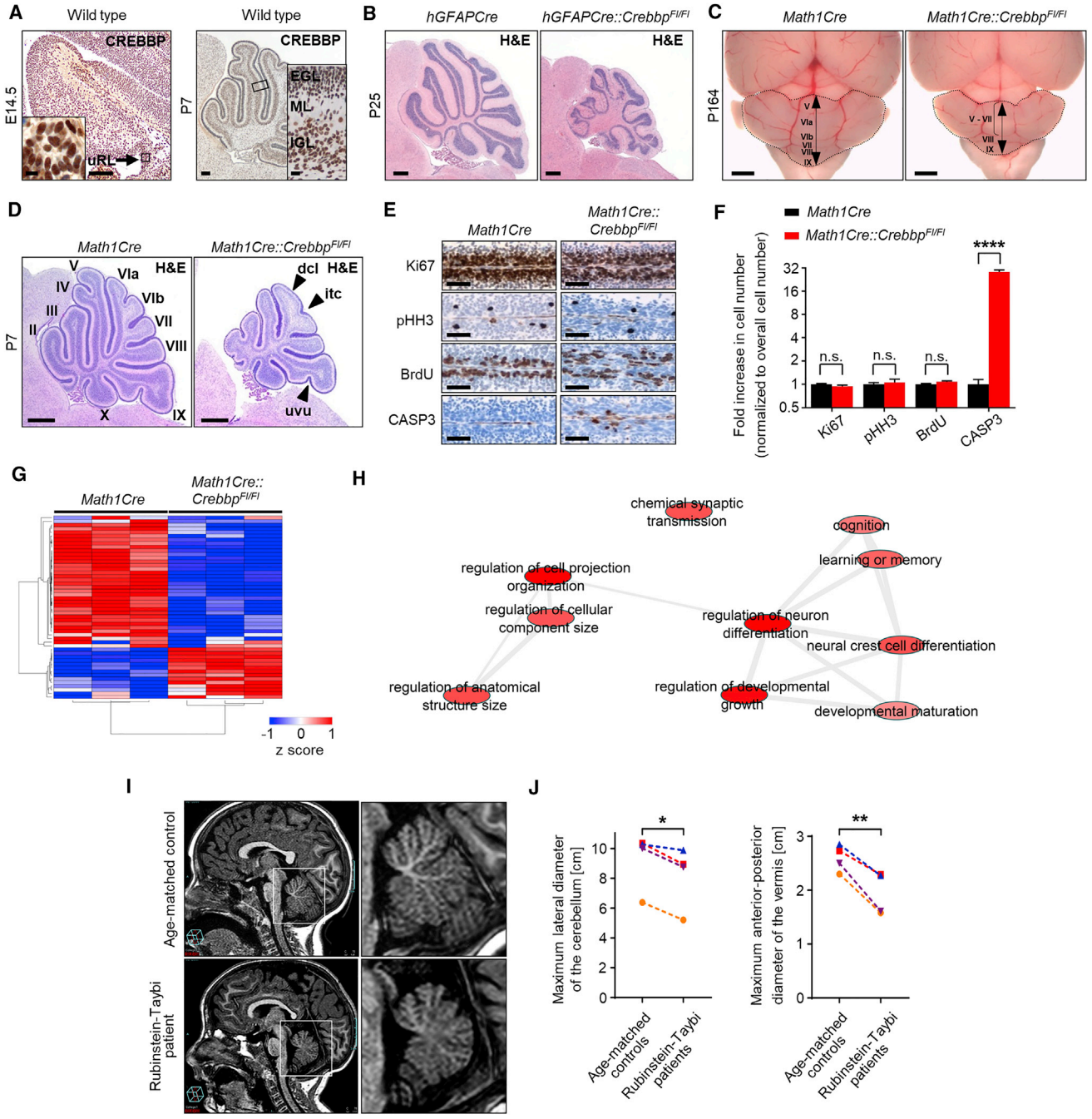

Figure 2. *Crebbp* Is Required for GNP Development and Normal Cerebellar Growth

(A) Immunohistochemistry for CREBBP in the murine cerebellum. The arrow points toward the upper rhombic lip. uRL, upper rhombic lip; EGL, external granule cell layer; ML, molecular layer; IGL, inner granule cell layer. Scale bar, 100 μm and 10 μm in insets.

(B) H&E staining of cerebella from *hGFAPCre* and *hGFAPCre::Crebbp*$^{Fl/Fl}$ mice at P25. Scale bar, 200 μm.

(C) Whole cerebella of *Math1Cre* and *Math1Cre::Crebbp*$^{Fl/Fl}$ mice at P164. Scale bar, 250 μm.

(D) H&E staining of cerebella from *Math1Cre* and *Math1Cre::Crebbp*$^{Fl/Fl}$ mice. The arrow heads point toward the declival sulcus (dcl), the intercrural fissure (itc), and the uvular sulcus (uvu). Scale bar, 250 μm.

(E) Immunohistochemistry for Ki67, phospho-histone H3 (pHH3), BrdU, and cleaved caspase-3 (CASP3) in the EGL of cerebella from *Math1Cre* and *Math1Cre::Crebbp*$^{Fl/Fl}$ mice. Scale bar, 40 μm.

(F) Quantification of markers shown in E in *Math1Cre::Crebbp*$^{Fl/Fl}$ mice compared with control mice (n = 5, unpaired t test).

(G) Unsupervised hierarchical clustering of the top 50 genes differentially expressed in P7 cerebella of *Math1Cre* and *Math1Cre::Crebbp*$^{Fl/Fl}$ mice (n = 3, Pearson correlation, average linkage).

(legend continued on next page)

2008) (Figure 2A). To determine, whether *Crebbp* inactivation leads to brain tumor formation, we generated *hGFAPCre::Crebbp*$^{Fl/Fl}$ mice in order to express a Crebbp N-terminal fragment (designated as *Crebbp* knockout) in a wide range of neural stem/progenitor cells that closely resembles CREBBP mutants found in human MB with stop gain mutations in the N-terminal part of the protein (Zhang et al., 2004; Zhuo et al., 2001). We observed an apparent cerebellar hypoplasia and disturbance of the cerebellar cortex structure in these mice, as well as significant lethality that was, however, not associated with any signs of tumor formation in the brain (Figures 2B and S2).

We next used GNP-restricted *Math1* promoter sequences to analyze *Crebbp* function in GNPs (Machold and Fishell, 2005). *Math1Cre::Crebbp*$^{Fl/Fl}$ mice showed significant lethality accompanied with a significant decrease in body weight and cerebellar mass (Figures S3A–S3C). Even though haploinsufficiency has been discussed as a possible mechanism during the development of RTS (Tanaka et al., 1997), we did not detect such abnormalities in *Math1Cre::Crebbp*$^{Fl/+}$ mice (Figure S3D). In contrast, analyses of *Math1Cre::Crebbp*$^{Fl/Fl}$ mice displayed cerebellar hypoplasia and disturbed foliation (Figures 2C and 2D). Specifically, the declival sulcus within folia VI, the intercrural fissure separating folia VI and VII, and the uvular sulcus within folia IX, were shallow or completely absent in mutant mice. Although *Math1* expression in GNP starts at embryonic day 13.5 (E13.5) (Wang et al., 2005), no morphological changes of the cerebellum or differences in proliferation and apoptosis in the nascent external granule cell layer (EGL) were seen at E16.5 (Figures S3E and S3F). At postnatal day 7 (P7), however, staining for cleaved caspase-3 revealed a significant increase in apoptotic GNPs, while proliferation was unaffected (Figures 2E and 2F).

We further performed gene expression profiling using Affymetrix Mouse Gene 2.0 ST arrays to look at global changes of gene expression after *Crebbp* knockout in cerebella of *Math1Cre::Crebbp*$^{Fl/Fl}$ mice at P7. Unsupervized hierarchical clustering (Figure 2G) revealed a high level of consistency across biological replicates (n = 3 cerebella per genotype). Using the criteria $|$ fold change $| \geq 1.5$ and adjusted $p < 0.05$, we found 158 genes to be differentially expressed (Table S2). Genes downregulated after *Crebbp* knockout included neuronal genes, such as *Cdh8* and *Neurod6*, which have been reported to be potential targets of the CREB transcription factor (Zhang et al., 2005). Subsequent gene ontology (GO) analyses revealed that almost all of the GO terms were predicted to be decreased in *Math1Cre::Crebbp*$^{Fl/Fl}$ mice, with GO terms indicative of developmental growth, cell differentiation, and neuronal projection/synapse development being highly inhibited by loss of *Crebbp*, which is in line with the severe cerebellar hypoplasia (Figure 2H; Table S3). Of note, among the most significantly affected GO terms by loss of *Crebbp* were *cognition* and *learning or memory*. Indeed, RTS patients are known to present severe cognitive impairment as well as difficulty in planning and executing motor acts (Hennekam et al., 1992; Gotts and Liemohn, 1977), further supporting the notion that this mouse model mirrors characteristics of RTS.

We further wanted to validate the findings from our mouse model in humans with a germline alteration of *CREBBP*. Representative magnetic resonance images from an RTS patient and an age-matched control indeed showed a mildly hypoplastic inferior vermis and callosal splenium in the RTS patient (Figure 2I). Further quantification of lateral as well as anterior-posterior cerebellar dimensions of a total of four RTS patients and corresponding age-matched controls substantiated this impression (Figure 2J), thereby mimicking the cerebellar phenotype seen in our mouse model. Taken together, early and chronic deletion of *Crebbp* interferes with GNP cell survival leading to cerebellar hypoplasia, and this feature can also be seen in patients with RTS.

Crebbp Expression in GNPs Acts Both in a Cell-Non-autonomous as well as an Autonomous Way

The process of cerebellar foliation is believed to be mainly orchestrated by anchoring centers, where GNPs, Bergmann glia (BG) fibers, and Purkinje cells (PCs) work together to form cerebellar fissures (Sudarov and Joyner, 2007). Since we saw defects in cerebellar foliation, we investigated these cell types in more detail. Surprisingly, even though *Math1* promoter sequences are described to be inactive in BG or PCs (Machold and Fishell, 2005), both cell types were affected by the loss of *Crebbp* in GNPs (Figure 3A). BG fibers developed bushy extensions in the EGL and did not form glial endfeet on the pial surface. Similarly, PC arborization was abnormal in *Math1Cre::Crebbp*$^{Fl/Fl}$ mice. In wild-type mice, a primary dendrite emanated from the cell body toward the pial surface, with small dendritic branches building a fine network within the molecular layer (ML). In contrast, mutant animals displayed a thickened dendrite emanating in random angles into the ML, lacking the fine dendritic network of wild-type animals. To ensure that our Cre driver was not activating Cre recombinase in PCs, we intercrossed a fate mapping *lacZ* allele by generating *Math1Cre::ROSA26lacZ*$^{Fl/+}$ mice. As expected, PCs were not stained by X-gal, indicating that *Math1* sequences in our mouse model were not active in PCs (Figure 3B). In addition to high apoptotic activity in GNPs from *Math1Cre::Crebbp*$^{Fl/Fl}$ mice, which is likely to contribute to the foliation deficits, these animals displayed GNP ectopia in adult cerebella, indicative of a migration defect of GNPs (Figures S4A and S4B). Indeed, a bromodeoxyuridine (BrdU) pulse experiment during early postnatal development supported this hypothesis (Figures S4C and S4D). While PAX6$^+$ cells in the ML during adulthood are a rare event in wild-type mice, the stalled PAX6$^+$ cells on the cerebellar surface or within the ML in mutant mice did not express CREBBP protein (Figure 3C). Of note, these ectopic cells stopped proliferating and did not go on to form tumors, as shown by the lack of Ki67 expression.

(H) Summarized GO terms regulated by chronic *Crebbp* expression in cerebellar GNPs where node color correlates with adjusted p value and edge width indicates the degree of similarity.

(I) IMR images displaying the sagittal plane from a Rubinstein-Taybi patient and an age-matched control.

(J) Statistical analysis of the maximal lateral diameter of the cerebellum ($p = 0.0189$) and the maximal anterior-posterior diameter of the vermis ($p = 0.0064$) from RTS patients and age-matched controls (n = 4, paired t test).

All graphs display mean ± SEM. *$p \leq 0.05$, **$p \leq 0.01$, ****$p \leq 0.001$. See also Figures S2 and S3.

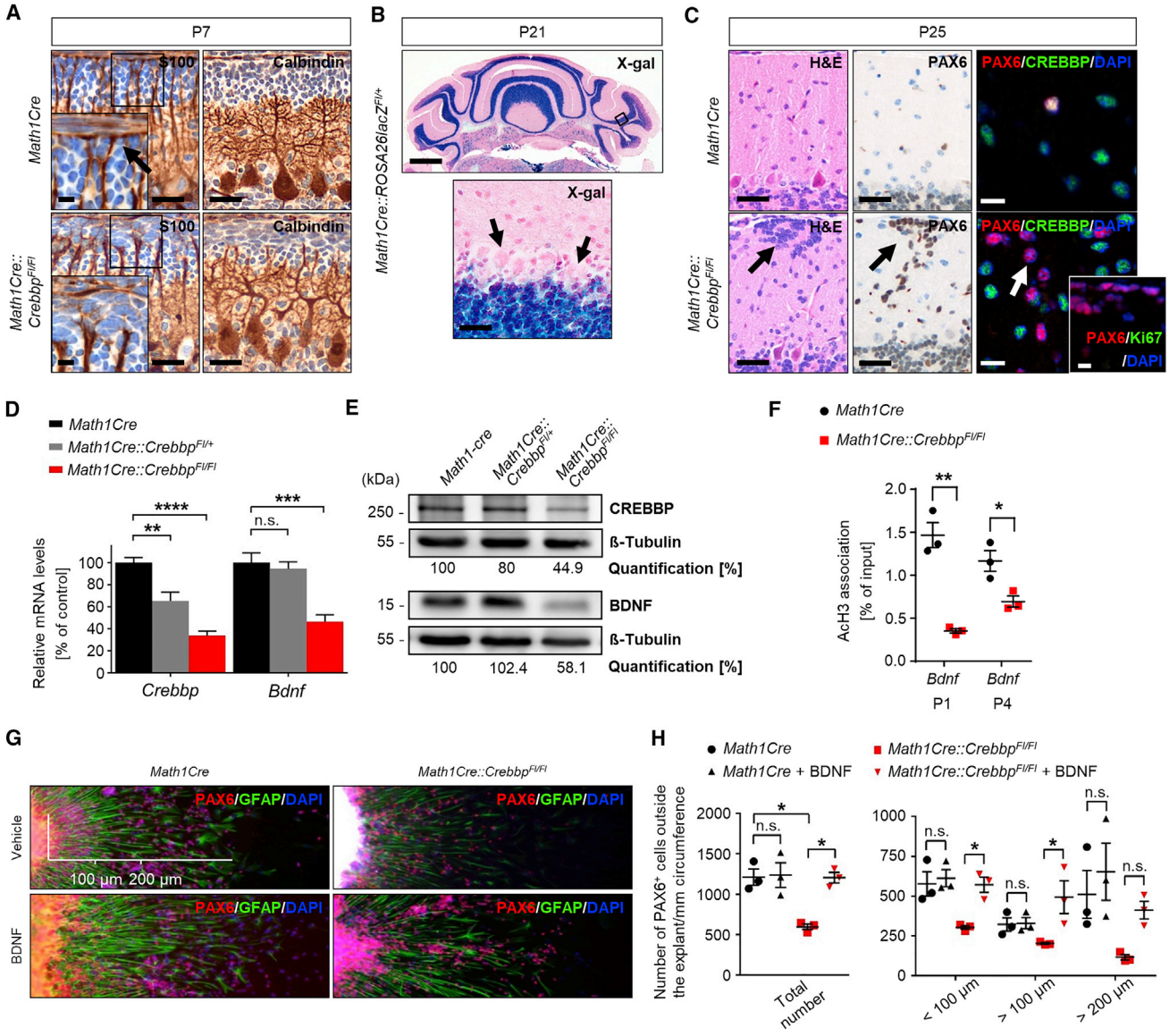

Figure 3. *Crebbp* Expression in GNPs Regulates Cerebellar Development by Cell Non-autonomous and Autonomous Mechanisms

(A) Immunohistochemistry for S100 and Calbindin of cerebella from *Math1Cre* and *Math1Cre::Crebbp*$^{Fl/Fl}$ mice. The arrow points toward glial endfeet. Scale bar, 30 µm, 10 µm in insets.

(B) X-gal staining of a cerebellum from a *Math1Cre::ROSA26lacZ*$^{Fl/+}$ mouse. The arrows point toward Purkinje cells. Scale bar, 500 µm, 50 µm in higher magnification.

(C) Representative H&E stainings and immunohistochemistry for PAX6, PAX6/CREBBP, and PAX6/Ki67 of cerebella from *Math1Cre* and *Math1Cre::Crebbp*$^{Fl/Fl}$ mice. The arrows point toward PAX6^{+} ectopic GNPs. Scale bars, 50 µm, 10 µm for co-stainings.

(D) qRT-PCR for *Crebbp* and *Bdnf* relative to *ß2m* in cerebella from P12 animals with indicated genotypes (n = 5, Bonferroni *post-hoc* test of one-way ANOVA).

(E) Western blot analysis using antibodies against CREBBP, BDNF, and β-tubulin in cerebellar protein lysates from mice with indicated genotypes.

(F) Chromatin immunoprecipitation analysis of *Bdnf* promoter regions P1 and P4 using a histone H3 pan-acetyl-specific antibody (n = 3, unpaired t test).

(G) Fluorescent immunohistochemistry for PAX6 and GFAP from cerebellar explant cultures from *Math1Cre* and *Math1Cre::Crebbp*$^{Fl/Fl}$ mice treated with vehicle or BDNF (200 ng/mL).

(H) Quantification of PAX6^{+} cells outside the explants relative to the circumference of the explant in mm (n = 3, Bonferroni *post-hoc* test of one-way ANOVA).

All graphs display mean ± SEM. *p ≤ 0.05, **p ≤ 0.01, ***p ≤ 0.001, ****p ≤ 0.0001. See also Figure S4.

It has been shown that expression of the neurotrophin, brain-derived neurotrophic factor (BDNF), is critical for GNP development, as it regulates GNP survival and serves both as a chemokinetic and chemotactic factor to organize GNP migration (Zhou et al., 2007; Choi et al., 2005; Borghesani et al., 2002). Indeed, *Bdnf* knockout mice resemble our *Math1Cre::Crebbp*$^{Fl/Fl}$ mice in several ways as they share (1) increased granule cell death, (2) abnormal cerebellar foliation, (3) deficits in GNP migration, and (4) abnormal PC arborization (Schwartz et al., 1997). We therefore investigated levels of *Bdnf* expression

in our mouse model at late postnatal stages, as *Bdnf* expression is known to increase during maturation (Puehringer et al., 2013). qRT-PCR at P12 indeed revealed a significant reduction of *Bdnf* levels in mutant mice (Figure 3D). Of note, *Bdnf* levels were unaffected in *Math1Cre::Crebbp*$^{Fl/+}$ mice, possibly explaining the lack of a cerebellar phenotype in these mice. Western blot analyses further confirmed the reduction of BDNF protein (Figure 3E). As CREBBP harbors HAT activity, reduced acetylation may be a possible mechanism for the reduced *Bdnf* expression levels that we observed in our mouse model. We therefore investigated the acetylation status of two promoter regions of *Bdnf* isoforms known to be expressed in the brain of the mouse (Aid et al., 2007). Chromatin immunoprecipitations for pan-acetylated histone H3 (AcH3) at these genomic loci showed a significant reduction of AcH3 association in mutant mice (Figure 3F), giving a mechanistic insight into the downregulation of *Bdnf* in these mice.

We further aimed at functionally investigating the contribution of *Bdnf* downregulation to the cerebellar phenotype seen in our mouse model by focusing on the impaired migration of GNPs. To do so, we first tested the ability of cerebellar explant cultures to recapitulate the impaired migration (Frick et al., 2012). Explant cultures from both *Math1Cre* and *Math1Cre::Crebbp*$^{Fl/Fl}$ mice developed a radial pattern of development with GFAP^{+} glial processes emanating from the explant and PAX6^{+} GNPs migrating along these extensions (Figure 3G). However, explants from mutant mice showed a significant decrease in the overall number of migrating GNPs as well as in the distance of GNP migration (Figure 3H). In order to test whether *Bdnf* downregulation might contribute to the impaired GNP migration, we added recombinant BDNF to explant cultures from control and mutant mice. Indeed, BDNF addition rescued the migration defect from mutant mice, both in terms of total numbers of GNPs migrating as well as the distance of migration covered by GNPs (Figures 3G and 3H). Together, these data suggest that *Crebbp*-dependent expression of *Bdnf* in the cerebellum is essential for normal development.

Chronic Loss of Crebbp Impairs Viability of GNP-Derived MB

While early loss of *Crebbp* in GNPs alone was not sufficient to induce tumor formation, we further analyzed both the impact of a heterozygous or homozygous *Crebbp* knockout in GNPs in an oncogenic setting by intercrossing an activated allele of *Smoothened* (*SmoM2*) (Grammel et al., 2012; Schüller et al., 2008). As before, analyses of our mouse models at E16.5 revealed no apparent effect of either a heterozygous or homozygous *Crebbp* knockout on overall tumor appearance, proliferation, and apoptosis, compared with wild-type *Crebbp* tumors (Figures 4A and 4B). However, at postnatal stage, GNP-derived tumor cells with a homozygous *Crebbp* knockout showed lower BrdU incorporation and increased apoptosis compared with wild-type tumors, while we did not detect those changes for tumors with a heterozygous loss of *Crebbp*. As the analysis of overall survival rates of these mice might be distorted by the primary lethality of *Math1Cre::Crebbp*$^{Fl/Fl}$ mice, we performed allogenic transplantations of tumor cells with either a homozygous or in-litter controls with a heterozygous *Crebbp* knockout into cerebella of wild-type mice and analyzed tumor development (Figure 4C). In line with our previous results, mice transplanted with tumor cells harboring a homozygous knockout of *Crebbp* displayed a significant reduction in tumor incidence (31.3%) compared with control mice (90.9%, Figure 4D). Also, mice transplanted with *Crebbp*-deficient tumor cells showed a significantly better overall survival (Figure 4E). Thus, *Crebbp* expression in embryonal GNPs does not convey tumor-suppressive functions. In fact, in a similar manner as during normal development, chronic loss of *Crebbp* induces apoptosis in GNP-derived Shh tumors.

Acute Loss of Crebbp at Postnatal Stage Interferes with GNP Cell-Cycle Exit

As *CREBBP* mutations in human SHH MBs show a clear preponderance in adult patients, we speculated that *Crebbp* tumor-suppressive functions in GNPs might be restricted to later developmental stages. In line with this hypothesis, acute deletion of *Crebbp* induced by Cre-encoding retroviral particles in GNP cultures of P5 *Crebbp*$^{Fl/Fl}$ mice significantly increased proliferation (Figures 5A and 5B). To validate these results *in vivo*, we generated *Math1CreER*^{T2}*::Crebbp*$^{Fl/Fl}$ (designated as *MCre*^{T2}*::Crebbp*) mice to specifically knockout *Crebbp* in postnatal GNPs by tamoxifen (TAM) injection at P5 (Figure 5C). While we did not observe an increase in apoptotic activity in GNPs in these mice after TAM treatment, acute loss of *Crebbp* at P5 was accompanied by a significant increase in proliferation of GNPs (Figures 5D and 5E). To validate our inducible mouse model, we also deleted *Crebbp* at different stages of embryonic development. While we did not see any apparent effect of *Crebbp* knockout at E18.5 when analyzed at P7, the knockout of *Crebbp* at E14.5 closely mimicked the situation seen after chronic *Crebbp* loss in *Math1Cre::Crebbp*$^{Fl/Fl}$ mice (Figure S5), suggesting that the differences in phenotype after chronic and acute *Crebbp* knockout are directly related to the stage of development of the GNPs.

We next analyzed cell-cycle duration in primary GNPs in response to loss of *Crebbp* by using an 5-ethynyl-2'-deoxyuridine (EdU)/BrdU double labeling approach. These analyses confirmed that cell-cycle duration of postnatal GNPs *in vitro* was not altered by loss of *Crebbp* (Figures 5F and 5G). In fact, GNPs with or without *Crebbp* knockout had a similar cell-cycle duration of about 20 hr, being well in line with previous data (Berenguer et al., 2013). To address, whether loss of *Crebbp* may inhibit cell-cycle exit of GNPs, we used sequential labeling of cells in S phase in *MCre*^{T2}*::Crebbp* and control mice treated with TAM. Of note, quantification showed a significantly higher fraction of GNPs re-entering the cell cycle after 20 hr in response to acute loss of *Crebbp* (Figures 5H and 5I). We therefore conclude that *Crebbp* expression contributes to cell-cycle exit of GNPs during postnatal development.

Crebbp Acts as a Tumor Suppressor at Late Stages of MB Initiation

We assumed that a failure to exit the cell cycle will cooperate with an oncogenic activation of Shh signaling specifically at postnatal stages, as supported by experiments on primary GNP cultures (Figures S6A and S6B). To test this hypothesis *in vivo*, we generated *Math1CreER*^{T2}*::Crebbp*$^{Fl/Fl}$*SmoM2-YFP*$^{Fl/+}$ (*MCre*^{T2}*::CrebbpSmoM2*) and *Math1CreER*^{T2}*::SmoM2-YFP*$^{Fl/+}$ (*MCre*^{T2}*::SmoM2*) mice and induced aberrant Shh

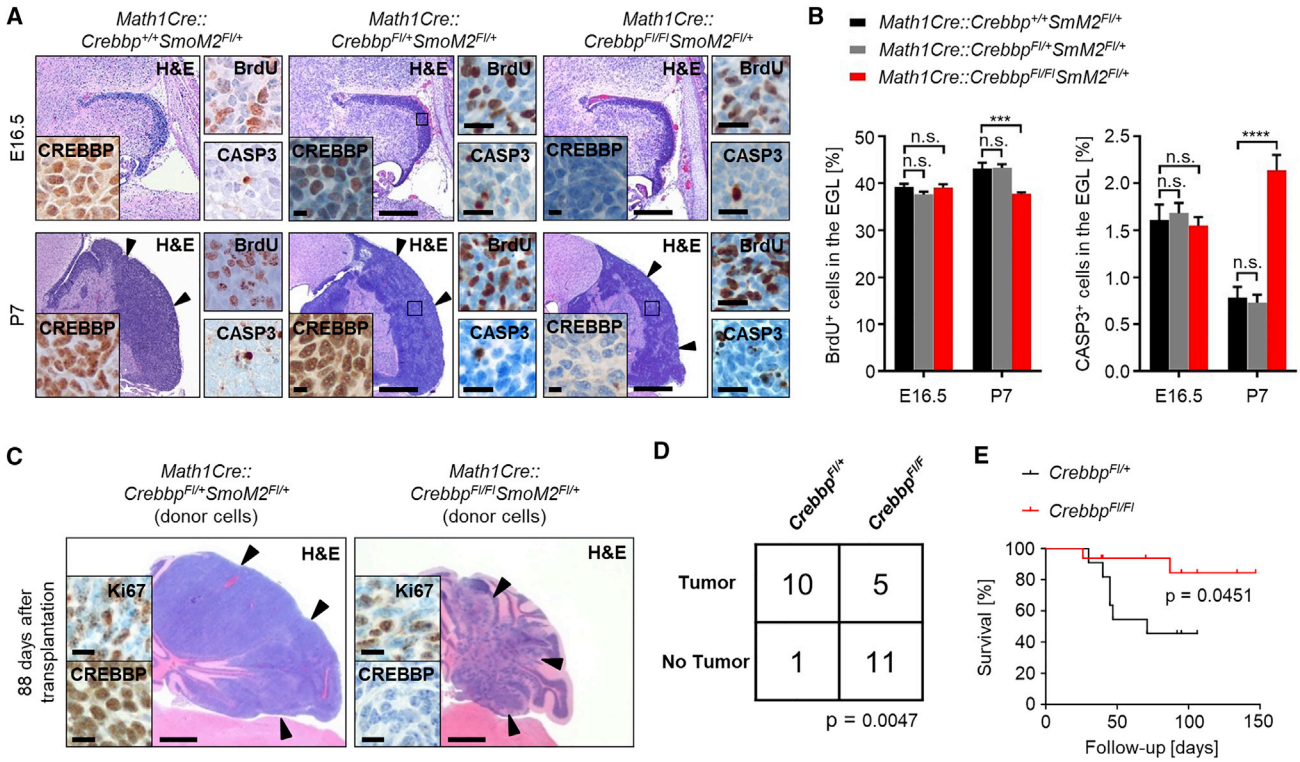

Figure 4. Chronic Loss of *Crebbp* Reduces Cell Viability of GNPs and SHH-Associated Medulloblastoma at Postnatal Stages

(A) H&E staining and immunohistochemistry for CREBBP, BrdU, and CASP3 in tumors from *Math1Cre::SmoM2*$^{Fl/+}$ mice with wild-type *Crebbp* (left), a heterozygous (middle), or a homozygous (right) deletion of *Crebbp*. Arrowheads illustrate tumor expansion. Scale bars, 200 μm, 10 μm in insets.

(B) Quantification of BrdU$^+$ cells and CASP3$^+$ cells in tumors from indicated mice (n = 5, Bonferroni *post-hoc* test of two-way ANOVA).

(C) H&E stainings and immunohistochemistry for Ki67 and CREBBP of brain sections after orthotopic transplantation of tumor cells derived from either *Math1Cre::Crebbp*$^{Fl/+}$*SmoM2*$^{Fl/+}$ or *Math1Cre::Crebbp*$^{Fl/Fl}$*SmoM2*$^{Fl/+}$ donor mice into cerebella of wild-type mice. Arrowheads illustrate tumor expansion. Scale bars, 500 μm, 10 μm in insets.

(D) Contingency table showing tumor incidence in transplanted tumor mouse models (Fisher's exact test).

(E) Survival analysis of transplanted tumor mouse models ($n_{CrebbpFl/+}$ = 11, $n_{CrebbpFl/Fl}$ = 16, Kaplan-Meier log rank test). Mice being asymptomatic at the time of preparation were included as censored.

All graphs display mean ± SEM. ***p ≤ 0.001, ****p ≤ 0.0001.

signaling by TAM induction at different stages during development (Figures 6A and 6B). Tumor induction at E14.5 supported our findings based on the *Math1Cre* driver line, with a clear increase in apoptotic activity and decrease in proliferation at postnatal stages in tumors with loss of *Crebbp*, while we did not see these differences when animals received TAM during late embryonic stage (E18.5) (Figures S6C and S6D). However, *MCre*^{T2}*::CrebbpSmoM2* mice treated with TAM at P5 displayed a thicker EGL and significantly more proliferating cells at P12 than *MCre*^{T2}*::SmoM2* mice. Consequently, these mice showed a significantly enhanced tumor growth and a reduced overall survival (Figure 6C). Of note, induced tumor mice with a heterozygous loss of *Crebbp* did not show any difference in terms of overall survival compared with *MCre*^{T2}*::SmoM2* mice (data not shown).

To test whether tumor-suppressive functions of *Crebbp* might be mediated by the expression of *Bdnf* in a similar way to the situation during embryonic development, we asked, whether *Bdnf* expression in postnatal GNPs might regulate Shh pathway and proliferation. Treatment of cultured GNPs with BDNF protein significantly reduced expression of *Ptch1* and *Gli1* (Figure S6E). In line with that, acute loss of *Bdnf* in cultured GNPs increased their proliferation both *in vitro* and *in vivo* (Figures S6F and S6G). We next determined whether *Bdnf* expression might be regulated by *Crebbp* in mouse MB. As shown by qRT-PCR and western blot, tumors with loss of *Crebbp* showed significantly lower levels of *Bdnf* expression (Figures 6D–6F). We then sought to determine if the acute loss of *Bdnf* might cooperate in a similar way with oncogenic Shh activation, as seen after acute loss of *Crebbp*. Analyses of *Math1Cre*^{T2}*::Bdnf*$^{Fl/Fl}$ *SmoM2-YFP*$^{Fl/+}$ (*MCre*^{T2}*::BdnfSmoM2*) mice 1 week after TAM induction at P5 revealed a thickening of the EGL during early tumor development, which was much more drastic than that seen in control tumor mice (Figure 6G). Also, BrdU pulse labeling showed a significant increase in proliferation in these mice compared with controls (Figure 6H), suggesting that loss of *Bdnf* enhanced tumor growth at this stage. To further validate whether *Bdnf* downregulation in these tumors is indeed responsible for aggressive tumor growth, we assessed the effect of BDNF treatment on proliferation of tumor cells with wild-type or loss of *Crebbp in vitro*. Indeed, BDNF treatment of cultured tumor cells from *MCre*^{T2}*::CrebbpSmoM2* mice significantly

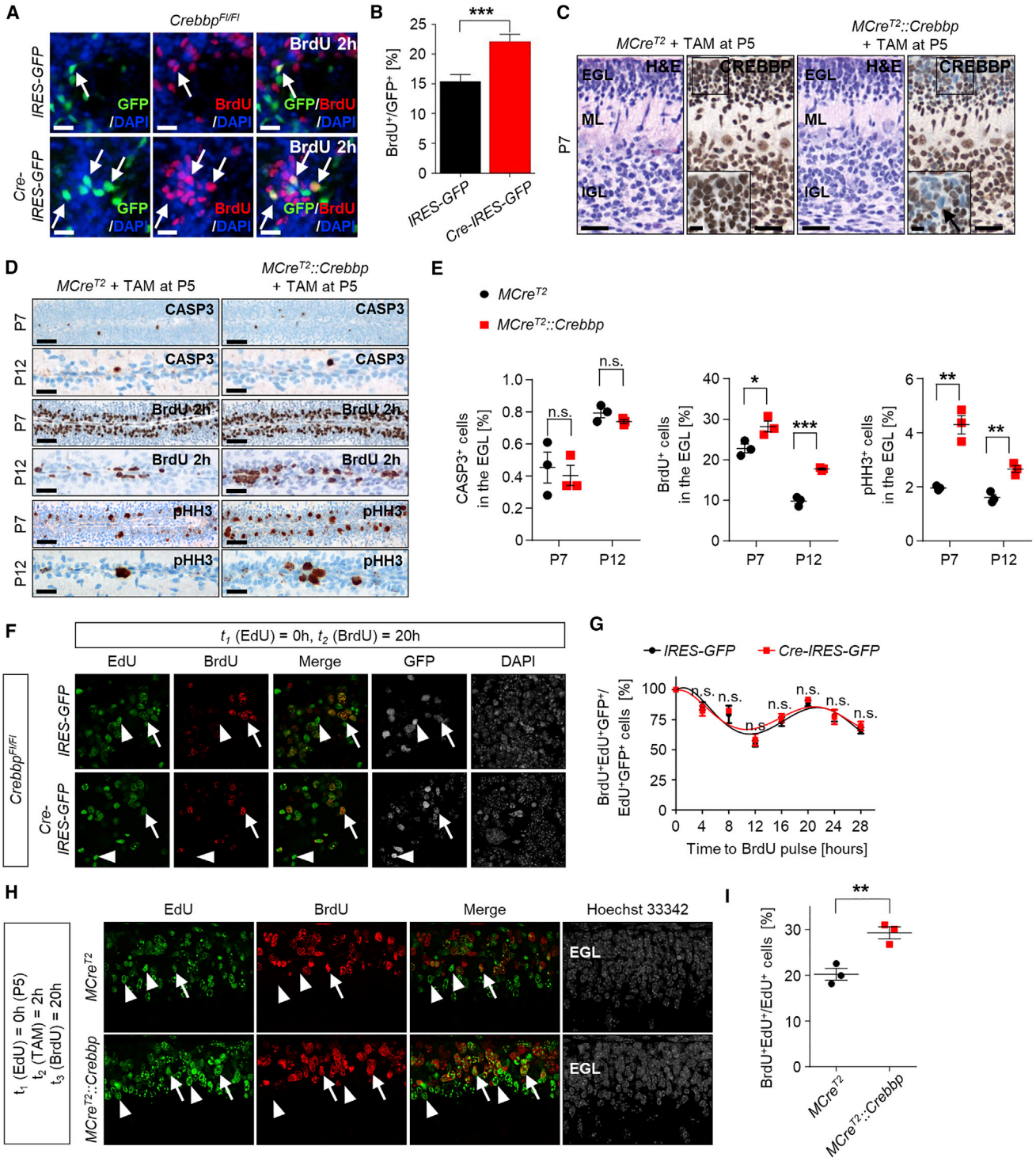

Figure 5. Acute Loss of *Crebbp* during Postnatal Development Enhances GNP Proliferation

(A) Cerebellar GNP cultures from P5 *Crebbp*$^{Fl/Fl}$ mice were transduced with indicated retroviruses and pulse labeled with BrdU. The arrows point toward BrdU$^+$/GFP$^+$ cells. Scale bar, 20 μm.

(B) Quantification of BrdU incorporation in cultures shown in (A) (n = 5, paired t test).

(C) H&E staining and immunohistochemistry for CREBBP of cerebella from *Math1CreER*^{T2} (*MCre*^{T2}) and *Math1CreER*^{T2}*::Crebbp*$^{Fl/Fl}$ (*MCre*^{T2}*::Crebbp*) mice treated with tamoxifen (TAM). The arrow in the inset points toward a CREBBP$^-$ cell in the EGL. Scale bars, 50 μm, 10 μm in insets. EGL, external granule cell layer; ML, molecular layer; IGL, inner granule cell layer.

(D) Immunohistochemistry for CASP3, BrdU, and pHH3 of TAM-induced *MCre*^{T2} and *MCre*^{T2}*::Crebbp* mice. Pictures show the EGL. Scale bar, 20 μm.

(legend continued on next page)

inhibited proliferation, whereas we did not observe a similar effect of BDNF on control tumor cells (Figures 6I and 6J). In addition, the effect of BDNF treatment was abrogated by the presence of TrkB-specific inhibitors ANA-12 and Cyclotraxin-B (Cazorla et al., 2011; Cazorla et al., 2010), suggesting that BDNF signaling via its cognate receptor TrkB is a downstream mechanism in Shh MBs with loss of *Crebbp*.

To gain further insights into the downstream effects of loss of *Crebbp* in MB, we again performed microarray analysis, which revealed 48 genes to be differentially expressed between tumors from *MCre^{T2}::SmoM2* and *MCre^{T2}::CrebbpSmoM2* mice (Figure 7A). While no enrichment of functional GO terms could be assigned to these genes at a significant level (data not shown), one of the genes upregulated in *Crebbp* knockout tumors was *Gli3*, a member of the Shh pathway (Table S4). qRT-PCR confirmed this upregulation, and revealed a substantial increase in mRNAs of *Gli1* and the direct *Gli1* target *Ptch1* (Agren et al., 2004) (Figure 7B). Consistent with this finding, protein levels of both GLI3 and GLI1 were significantly elevated after loss of *Crebbp* in postnatally induced tumors (Figures 7C and 7D), being well in line with the fact that *Gli1* is a direct transcriptional target of *Gli3* (Dai et al., 1999). By contrast, loss of *Crebbp* in embryonically induced tumors was associated with lower GLI3/GLI1 levels. These data suggest that loss of *Crebbp* in late-stage tumors directly enhances oncogenic Shh signaling via regulation of Gli effectors.

To extend these observations to patient-derived tumors, we conducted RNA sequencing for two independent tumor cohorts of adult SHH MBs and performed differential gene expression analysis. In doing so, we identified a total of 154 genes (Heidelberg cohort) and 166 genes (Toronto cohort) as being differentially expressed (Table S5). Of note, while only four genes were present in both gene lists, the expression of differentially expressed genes positively correlated across both tumor cohorts (Figure S7). Interestingly, none of the SHH components found to be upregulated in the mouse tumors with *Crebbp* knockout were seen to be upregulated in human tumors with *CREBBP* mutation at a significant level. However, gene set enrichment analysis, which was used to look for co-ordinated changes in well-defined gene sets, identified E2F signaling, a pathway downstream of Shh signaling in GNPs and implicated in MB formation (Olson et al., 2007; Marino et al., 2003; Oliver et al., 2003), as well as SHH signaling itself as top signatures enriched in tumors with *CREBBP* mutation consistent across both cohorts (Figure 7E; Table S6). Further functional annotation of recurrent leading-edge genes from signatures significantly enriched in either *CREBBP* wild-type or mutation cases across cohorts (Table S7) revealed top GO terms from cases with *CREBBP* mutation to be associated with DNA replication, mitosis, or cell-cycle regulation, all functional categories that have been shown to be positively regulated by Shh in GNPs (Oliver et al., 2003). In contrast, GO terms enriched in *CREBBP* wild-type cases were linked with neuron-associated functions such as synaptic signaling. These data suggest that *CREBBP* alterations in both murine and human MB foster tumor growth by enhancing SHH output.

DISCUSSION

Mutations in genes coding for chromatin modifiers are frequent in adult SHH MB (Kool et al., 2014), However, it is still unclear how these mutations contribute to tumor development and growth. We report here on opposing effects of *CREBBP* mutations during cerebellar development that underlie both the pathogenesis of RTS-associated cerebellar malformations and the development of adult SHH MB.

Germline mutations of *CREBBP* are associated with the developmental disorder RTS (Giles et al., 1997; Petrij et al., 1995). Apart from the known predisposition for cancer development, increasing evidence suggests that cerebellar malformations such as hypoplasia and Dandy-Walker-like alterations are frequent findings in RTS (Greco et al., 2009; Bonioli et al., 1989). These observations perfectly match the impaired cerebellar development in our model system with chronic *Crebbp* knockout, as well as the cerebellar phenotype seen in MRIs of RTS patients. Our data suggest that persistent expression of *Crebbp* throughout development governs a transcriptional network that enables GNPs to survive and differentiate during postnatal development. We further provide evidence that the complex phenotype seen in our mouse model is in part due to a deregulation of the neurotrophin Bdnf. Indeed, a *Crebbp*-dependent regulation of *Bdnf* expression has been suggested in several biological contexts (Zhu et al., 2014; Caccamo et al., 2010). However, seeing the much more severe phenotype in our mice compared with *Bdnf* knockout mice, it seems likely that other additional mechanisms are involved in the pathogenesis following loss of *Crebbp*. Further studies are needed to fully investigate these alterations. Of note, while haploinsufficient mechanisms are believed to lead to RTS (Tanaka et al., 1997; Petrij et al., 1995), our data suggest that *Crebbp* does not act in a haploinsufficient manner in murine GNPs or GNP-derived mouse tumors, being well in line with more recent reports (Wu et al., 2012; Kung et al., 2000). While this might seem to disagree with heterozygous *CREBBP* mutations in RTS and MB patients, we provide *in vitro* evidence that at least some SHH MB-associated CREBBP mutants act in a dominant-negative manner, being well in line with observations of dominant-negative forms of CREBBP protein in mouse models (Oike et al., 1999). Together,

(E) Quantification of CASP3$^+$, BrdU$^+$, and pHH3$^+$ cells in TAM-induced *MCre^{T2}* and *MCre^{T2}::Crebbp* mice (n = 3, unpaired t test).
(F) GNP cultures from P5 *Crebbp$^{Fl/Fl}$* mice were transduced with indicated retroviruses and consecutively labeled with EdU and BrdU to determine cell-cycle duration. Pictures are shown for BrdU pulse applied 20 hr after EdU pulse. The arrowheads depict EdU$^+$ cells, the arrows BrdU$^+$EdU$^+$ cells. Scale bar, 10 μm.
(G) Quantification of the number of BrdU$^+$EdU$^+$GFP$^+$ cells in the EdU$^+$GFP$^+$ cell population in transduced GNPs (n = 3, paired t test).
(H) Double pulse labeling with EdU and BrdU in *MCre^{T2}* and *MCre^{T2}::Crebbp* mice. The arrowheads depict EdU$^+$ cells, the arrows BrdU$^+$EdU$^+$ cells. Scale bar, 10 μm.
(I) Quantification of BrdU$^+$ cells in the EdU$^+$ cell population in the EGL of *MCre^{T2}* and *MCre^{T2}::Crebbp* mice after treatment regimen shown in (F) (n = 3, unpaired t test).
All graphs display mean ± SEM. *p ≤ 0.05, **p ≤ 0.01, ***p ≤ 0.001. See also Figure S5.

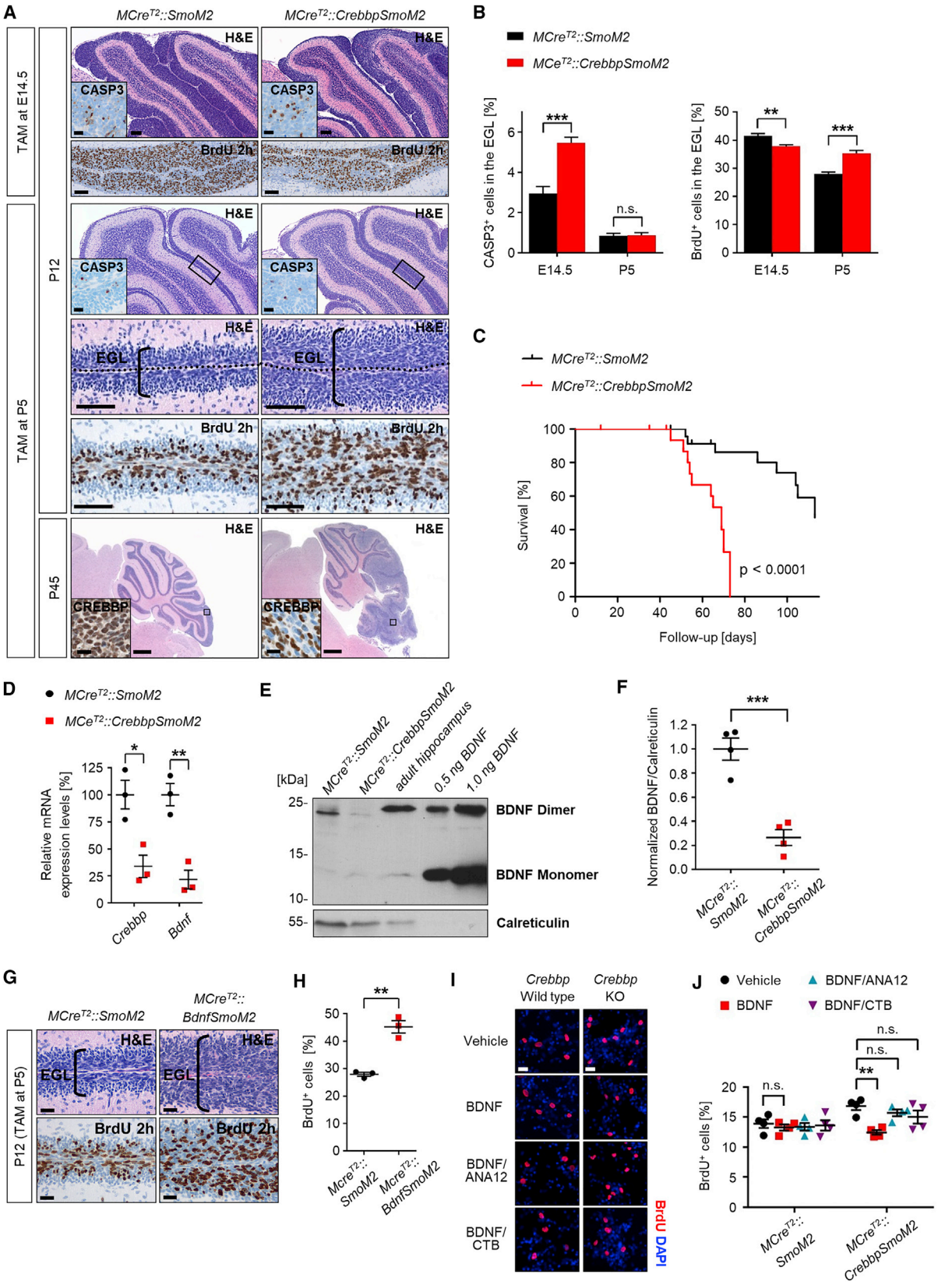

(legend on next page)

the ability of a specific CREBBP mutant to act as a dominant-negative effector, as well as the susceptibility of a given cell type to haploinsufficiency of *CREBBP*, is likely to explain the variety of phenotype penetrance in RTS, and our data add to this by showing that Crebbp does not act in a haploinsufficient manner during cerebellar development.

Even though only a very limited number of MBs from RTS patients have been described in more detail, it seems that these tumors are not necessarily SHH tumors arising in adults. In fact, reported cases occurred in children (Miller and Rubinstein, 1995), and a more recent report (as well as our own unpublished data) suggest that these tumors represent group 3 or group 4 MB (Bourdeaut et al., 2014). While these observations in RTS patients appear not to fit to the findings in sporadic MBs, they fit well to our findings that chronic ablation of *Crebbp* rather antagonizes the development of Shh MBs from GNPs. In fact, they support the hypothesis that group 3 and 4 MBs do not originate from hemispheric GNPs (Lin et al., 2016), and underline that the role of *CREBBP* mutations for group 3 and 4 MB needs to be investigated in future studies.

The tumor-suppressive functions of *Crebbp* restricted to late-stage granule neuron development are well in line with the preferred occurrence of *CREBBP* mutations in adult SHH MBs and suggest that the demography of patients with SHH MBs is directly associated with the developmental stage of GNPs at tumor initiation. This hypothesis further matches our previous data, showing that Shh MB formation from postnatal GNPs in mice is primarily restricted to the cerebellar hemispheres, the most prevalent location of SHH MBs in adult patients (Ohli et al., 2015; Wefers et al., 2014). Mechanistically, we show here that a *Crebbp*-dependent regulation of *Bdnf* at least in part is responsible for the tumor-suppressive functions of *Crebbp* during postnatal development. While most studies assign an oncogenic role to its expression, BDNF might also act as a tumor suppressor depending on the tumor entity (Huth et al., 2014; Au et al., 2009; Li et al., 2007). While our data show that BDNF acts as a tumor suppressor in GNPs and GNP-derived MB, it is not clear whether this is due to direct action of BDNF on the SHH pathway, or merely a secondary effect of BDNF-induced differentiation. This needs to be investigated in future studies.

Intriguingly, *Gli3*, a member of the Shh pathway was identified to be significantly upregulated in postnatally induced, *Crebbp*-deficient tumors. GLI3 has been shown previously to directly interact with CREBBP, and while CREBBP hereby acts as a co-activator, full-length GLI3 independently of CREBBP shows substantial transcriptional activation of downstream targets such as *Gli1* (Dai et al., 1999). The similarity between RTS and syndromes caused by *GLI3* mutations, such as Pallister-Hall syndrome, suggest that the biochemical interaction between CREBBP and GLI3 may influence SHH signaling (Cohen, 2010), and this is supported by our data showing that increased *Gli3* expression due to acute loss of *Crebbp* correlates with higher GLI1 protein levels. Furthermore, transcriptional profiling revealed an enrichment of target genes from SHH and E2F in human SHH MBs with *CREBBP* mutation, implying that loss of *CREBBP* in these tumors enhances SHH output. Of note, neither expression of *GLI3* and *GLI1* nor H3K27 acetylation at these loci as determined by chromatin immunoprecipitation sequencing were found to be significantly altered in SHH MBs with *CREBBP* mutation (data not shown). While this seemingly does not fit to the results found in our mouse model, this is not surprising given the fact that most adult SHH MBs harbor mutations in other chromatin modifiers, which might fulfill similar functions as *CREBBP*. For instance, mutations affecting the SWI-SNF complex, such as *ARID1B, SMARCA2*, or *SMARCB1*, may be seen in these tumors (Kool et al., 2014), and alterations of the latter have recently been described to drive *GLI1* overexpression and SHH signaling activation in malignant rhabdoid tumors (Jagani et al., 2010). In this way, our mouse model might reflect a direct function of *CREBBP* that is not obscured by the effects of other mutations modifying the genomic landscape of human MBs.

In conclusion, we found that chronic biallelic inactivation of *Crebbp* in GNPs leads to cerebellar hypoplasia, a phenotype that we show is also seen in patients with RTS. Also, we defined a late temporal window of GNP development, during which loss of *Crebbp* synergizes with Shh signaling to enhance pathway output and drive tumor growth. Further study is needed to investigate the precise role of individual mutations in chromatin-modifying genes in the development of MB, and whether or not these mutations might represent vulnerabilities that can be targeted to treat individual tumors.

Figure 6. *Crebbp* Acts as a Tumor Suppressor at Late Stages of Medulloblastoma Initiation

(A) *Math1CreER^{T2}::SmoM2$^{Fl/+}$* (*MCre^{T2}::SmoM2*) and *Math1CreER^{T2}::Crebbp$^{Fl/Fl}$SmoM2$^{Fl/+}$* (*MCre^{T2}::CrebbpSmoM2*) mice were induced with tamoxifen (1 mg) at E14.5 or P5 and subsequently pulse labeled at P12 with BrdU for 2 hr. H&E staining and immunohistochemistry for CASP3 (insets), BrdU, and CREBBP of the EGL. Additional stainings after TAM induction at P5 are shown for P45. Scale bars, 250 μm at P45, others 50 μm, 10 μm in insets.

(B) Quantification of CASP3$^+$ and BrdU$^+$ cells in the EGL of *MCre^{T2}::SmoM2* and *MCre^{T2}::CrebbpSmoM2* mice at P12, with TAM induction at E14.5 or P5 (n = 5, unpaired t test).

(C) Kaplan-Meier curves showing overall survival of *MCre^{T2}::SmoM2* (n = 25) compared with tumor mice with homozygous loss of Crebbp (*MCre^{T2}::CrebbpSmoM2*, n = 26) after tamoxifen induction at P5 (log rank test). Mice being asymptomatic at the time of preparation were included as censored.

(D) qRT-PCR analysis for *Crebbp* and *Bdnf* relative to *ß2m* in tumors from *MCre^{T2}::SmoM2* and *MCre^{T2}::CrebbpSmoM2* mice (n = 3, unpaired t test).

(E) Representative western blot images for BDNF and calreticulin in tumors from *MCre^{T2}::SmoM2* and *MCre^{T2}::CrebbpSmoM2* mice. A protein lysate from adult hippocampus and recombinant human BDNF were run along as controls.

(F) Densitometric quantification of BDNF protein levels in tumors with or without loss of *Crebbp* relative to calreticulin. (n = 4, unpaired t test).

(G) H&E staining and immunohistochemistry for BrdU for *MCre^{T2}::SmoM2* and *MCre^{T2}::BdnfSmoM2* mice that were induced with TAM (1 mg) at P5 and pulse labeled at P12 for 2 hr. Scale bars, 25 μm.

(H) Quantification shows fraction of BrdU$^+$ cells in the EGL (n = 3, unpaired t test).

(I) Tumor cells from *MCre^{T2}::SmoM2* and *MCre^{T2}::CrebbpSmoM2* mice were cultured *in vitro* and treated with vehicle, BDNF (200 ng/mL) alone or in combination with the TrkB inhibitors ANA-12 (1 μM) or cyclotraxin-B (CTB) (200 nM) for 24 hr. Scale bars, 10 μm.

(J) Quantification of the fraction of BrdU$^+$ cells in cultured tumor cells with the treatment regimen shown in (I) (n = 4, paired t test).

All graphs display mean ± SEM. *p ≤ 0.05, **p ≤ 0.01, ***p ≤ 0.001. See also Figure S6.

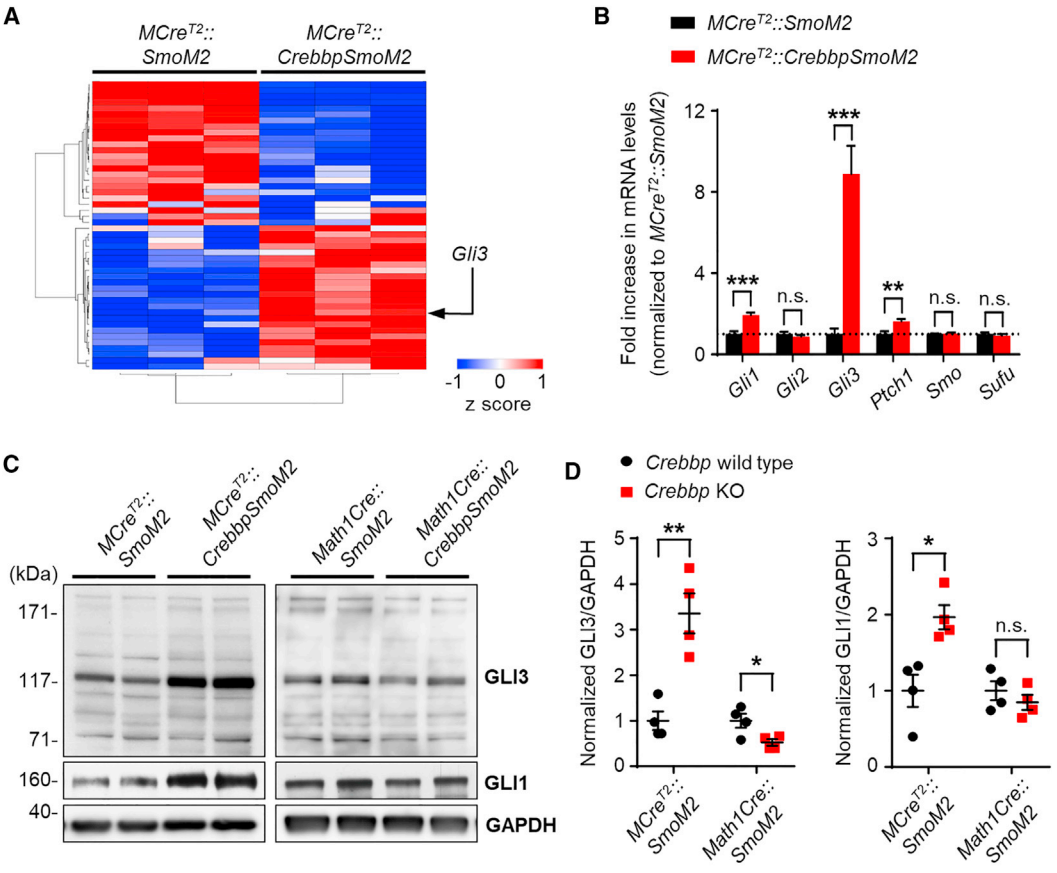

(legend on next page)

STAR★METHODS

Detailed methods are provided in the online version of this paper and include the following:

- KEY RESOURCES TABLE
- CONTACT FOR REAGENT AND RESOURCE SHARING
- EXPERIMENTAL MODEL AND SUBJECT DETAILS
  - Mice
  - Cell Culture
  - Primary Cell Cultures
- METHOD DETAILS
  - Mice Treatments
  - Orthotopic Transplantation of Tumor Cells
  - Pulse Labeling GNP Cultures
  - Production of Retroviral Particles
  - Generation of FLAG-Tagged CREBBP Mutants
  - Isolation of Recombinant FLAG-Tagged Proteins
  - Protein Structures and *In Vitro* Acetylation Assay
  - Generation of Stable HEK293T CREBBP Clones
  - Analysis of Histone Acetylation
  - Immunohistochemistry and Image Quantification
  - X-gal Stainings
  - Immunocytochemistry
  - Western Blot Analysis
  - Quantitative Real Time PCR (qRT-PCR)
  - Chromatin Immunoprecipitations
  - Microarray and Gene Ontology Analysis
  - Sequencing of Human Tumor Samples
  - RNA-Seq and Differential Gene Expression Analysis
  - Gene Set Enrichment Analysis (GSEA)
  - Publication Consent for Human Data
- QUANTIFICATION AND STATISTICAL ANALYSIS
- DATA AND SOFTWARE AVAILABILITY

SUPPLEMENTAL INFORMATION

Supplemental Information includes seven figures and seven tables and can be found with this article online at https://doi.org/10.1016/j.devcel.2018.02.012.

ACKNOWLEDGMENTS

We are indebted to Michael Schmidt, Silvia Occhionero, Marie-Christin Burmester, and Veronika Kaltenbrunn for excellent technical support, the Transcriptome and Genome Analysis Laboratory at the University Medical Center for microarray analysis, as well as expert assistance of the technical staff of the Molecular Genetics Lab of the Institute of Human Genetics Kiel. We also thank K. Hartmann from the mouse pathology core facility (UKE Hamburg, Germany) for processing immunohistochemical stainings. This work was supported by grants from the German Cancer Aid, the Wilhelm Sander-Stiftung, and the Fördergemeinschaft Kinderkrebs-Zentrum Hamburg. The MAGIC project acknowledges financial support from Genome Canada, Genome BC, Terry Fox Research Institute, Ontario Institute for Cancer Research, Pediatric Oncology Group Ontario, Funds from "The Family of Kathleen Lorette" and the Clark H. Smith Brain Tumour Centre, Montreal Children's Hospital Foundation, Hospital for Sick Children: Sonia and Arthur Labatt Brain Tumour Research Centre, Chief of Research Fund, Cancer Genetics Program, Garron Family Cancer Centre, and B.R.A.I.N. Child. We also acknowledge grant support for infrastructure by the KinderKrebsInitiative Buchholz/Holm-Seppensen.

AUTHOR CONTRIBUTIONS

Conceptualization, D.J.M. and U.S.; Methodology, D.J.M. and U.S.; Formal Analysis, D.J.M., N.D.M., V.T., S.M., and T.A.; Investigation, D.J.M., J.O., N.D.M., V.T., S.M., S.N.S., L.H., S.F., J.A., M. Schoof, S.E., K.R., T.A., M.W., M.L., J.E.N., M. Shakarami, D.P., M.A.M., Y.L., A.J.M., R.A.M., Y.M., S.J.M.J., B.E.-W., A.R., R.W., R.S., and A.J.; Resources, B. Lutz, B.E.-W., A.R., C.G.E., B. Lach, M. Sendtner, S.M.P., M.D.T., L.C., M.K., and U.S.; Writing – Original Draft, D.J.M. and U.S.; Writing – Review & Editing, D.J.M. and U.S.; Visualization, D.J.M. and U.S.; Funding Acquisition, D.J.M. and U.S.; Supervision, D.J.M. and U.S.

DECLARATION OF INTERESTS

The authors declare no competing interests.

Received: October 6, 2017
Revised: January 8, 2018
Accepted: February 12, 2018
Published: March 15, 2018

REFERENCES

Agren, M., Kogerman, P., Kleman, M.I., Wessling, M., and Toftgard, R. (2004). Expression of the PTCH1 tumor suppressor gene is regulated by alternative promoters and a single functional Gli-binding site. Gene *330*, 101–114.

Aguado, T., Romero, E., Monory, K., Palazuelos, J., Sendtner, M., Marsicano, G., Lutz, B., Guzman, M., and Galve-Roperh, I. (2007). The CB1 cannabinoid receptor mediates excitotoxicity-induced neural progenitor proliferation and neurogenesis. J. Biol. Chem. *282*, 23892–23898.

Aid, T., Kazantseva, A., Piirsoo, M., Palm, K., and Timmusk, T. (2007). Mouse and rat BDNF gene structure and expression revisited. J. Neurosci. Res. *85*, 525–535.

Au, C.W., Siu, M.K., Liao, X., Wong, E.S., Ngan, H.Y., Tam, K.F., Chan, D.C., Chan, Q.K., and Cheung, A.N. (2009). Tyrosine kinase B receptor and BDNF expression in ovarian cancers - effect on cell migration, angiogenesis and clinical outcome. Cancer Lett. *281*, 151–161.

Berenguer, J., Herrera, A., Vuolo, L., Torroba, B., Llorens, F., Sumoy, L., and Pons, S. (2013). MicroRNA 22 regulates cell cycle length in cerebellar granular neuron precursors. Mol. Cell. Biol. *33*, 2706–2717.

Bonioli, E., Bellini, C., and Di Stefano, A. (1989). Unusual association: Dandy-Walker-like malformation in the Rubinstein-Taybi syndrome. Am. J. Med. Genet. *33*, 420–421.

Figure 7. Loss of *Crebbp* at Late Stages of Medulloblastoma Initiation Enhances Shh Signaling

(A) Unsupervied hierarchical clustering of differentially expressed genes in tumors from *MCre^{T2}::SmoM2* and *MCre^{T2}::CrebbpSmoM2* mice (n = 3, Pearson correlation, average linkage).

(B) qRT-PCR quantification of Shh pathway components in tumors from *MCre^{T2}::SmoM2* and *MCre^{T2}::CrebbpSmoM2* mice (n = 6, unpaired t test).

(C) Representative western blot images for GLI3, GLI1, and glyceraldehyde-3-phosphate dehydrogenase (GAPDH) from postnatally (left) and embryonically induced tumors (right) with or without *Crebbp* knockout.

(D) Densitometric quantification of full-length GLI3 and GLI1 protein levels in tumors induced postnatally or embryonically relative to GAPDH (n = 4, unpaired t test).

(E) Gene set enrichment analysis enrichment score plots for human SHH MBs showing positive correlation between genes induced by *CREBBP* mutation and genes associated with active E2F and SHH signaling and negative correlation with genes from the KRAS.KIDNEY_UP.V1_UP gene set.

All graphs display mean ± SEM. *p ≤ 0.05, **p ≤ 0.01, ***p ≤ 0.001. See also Figure S7.

Borghesani, P.R., Peyrin, J.M., Klein, R., Rubin, J., Carter, A.R., Schwartz, P.M., Luster, A., Corfas, G., and Segal, R.A. (2002). BDNF stimulates migration of cerebellar granule cells. Development *129*, 1435–1442.

Bourdeaut, F., Miquel, C., Richer, W., Grill, J., Zerah, M., Grison, C., Pierron, G., Amiel, J., Krucker, C., Radvanyi, F., et al. (2014). Rubinstein-Taybi syndrome predisposing to non-WNT, non-SHH, group 3 medulloblastoma. Pediatr. Blood Cancer *61*, 383–386.

Caccamo, A., Maldonado, M.A., Bokov, A.F., Majumder, S., and Oddo, S. (2010). CBP gene transfer increases BDNF levels and ameliorates learning and memory deficits in a mouse model of Alzheimer's disease. Proc. Natl. Acad. Sci. USA *107*, 22687–22692.

Cazorla, M., Jouvenceau, A., Rose, C., Guilloux, J.P., Pilon, C., Dranovsky, A., and Premont, J. (2010). Cyclotraxin-B, the first highly potent and selective TrkB inhibitor, has anxiolytic properties in mice. PLoS One *5*, e9777.

Cazorla, M., Premont, J., Mann, A., Girard, N., Kellendonk, C., and Rognan, D. (2011). Identification of a low-molecular weight TrkB antagonist with anxiolytic and antidepressant activity in mice. J. Clin. Invest. *121*, 1846–1857.

Cho, Y.-J., Tsherniak, A., Tamayo, P., Santagata, S., Ligon, A., Greulich, H., Berhoukim, R., Amani, V., Goumnerova, L., Eberhart, C.G., et al. (2011). Integrative genomic analysis of medulloblastoma identifies a molecular subgroup that drives poor clinical outcome. J. Clin. Oncol. *29*, 1424–1430.

Choi, Y., Borghesani, P.R., Chan, J.A., and Segal, R.A. (2005). Migration from a mitogenic niche promotes cell-cycle exit. J. Neurosci. *25*, 10437–10445.

Cohen, M.M., Jr. (2010). Hedgehog signaling update. Am. J. Med. Genet. A *152A*, 1875–1914.

Dai, P., Akimaru, H., Tanaka, Y., Maekawa, T., Nakafuku, M., and Ishii, S. (1999). Sonic hedgehog-induced activation of the Gli1 promoter is mediated by GLI3. J. Biol. Chem. *274*, 8143–8152.

Dobin, A., Davis, C.A., Schlesinger, F., Drenkow, J., Zaleski, C., Jha, S., Batut, P., Chaisson, M., and Gingeras, T.R. (2013). STAR: ultrafast universal RNA-seq aligner. Bioinformatics *29*, 15–21.

Frick, A., Grammel, D., Schmidt, F., Pöschl, J., Priller, M., Pagella, P., von Bueren, A.O., Peraud, A., Tonn, J.-C., Herms, J., et al. (2012). Proper cerebellar development requires expression of β1-integrin in Bergmann glia, but not in granule neurons. Glia *60*, 820–832.

Giles, R.H., Petrij, F., Dauwerse, H.G., den Hollander, A.I., Lushnikova, T., van Ommen, G.J., Goodman, R.H., Deaven, L.L., Doggett, N.A., Peters, D.J., et al. (1997). Construction of a 1.2-Mb contig surrounding, and molecular analysis of, the human CREB-binding protein (CBP/CREBBP) gene on chromosome 16p13.3. Genomics *42*, 96–114.

Gotts, E.E., and Liemohn, W.P. (1977). Behavioral characteristics of three children with the broad thumb-hallux (Rubinstein-Taybi) syndrome. Biol. Psychiatry *12*, 413–423.

Grammel, D., Warmuth-Metz, M., von Bueren, A.O., Kool, M., Pietsch, T., Kretzschmar, H.A., Rowitch, D.H., Rutkowski, S., Pfister, S.M., and Schüller, U. (2012). Sonic hedgehog-associated medulloblastoma arising from the cochlear nuclei of the brainstem. Acta Neuropathol. *123*, 601–614.

Greco, E., Sglavo, G., and Paladini, D. (2009). Prenatal sonographic diagnosis of Rubinstein-Taybi syndrome. J. Ultrasound Med. *28*, 669–672.

Hennekam, R.C., Baselier, A.C., Beyaert, E., Bos, A., Blok, J.B., Jansma, H.B., Thorbecke-Nilsen, V.V., and Veerman, H. (1992). Psychological and speech studies in Rubinstein-Taybi syndrome. Am. J. Ment. Retard. *96*, 645–660.

Hovestadt, V., Remke, M., Kool, M., Pietsch, T., Northcott, P.A., Fischer, R., Cavalli, F.M., Ramaswamy, V., Zapatka, M., Reifenberger, G., et al. (2013). Robust molecular subgrouping and copy-number profiling of medulloblastoma from small amounts of archival tumour material using high-density DNA methylation arrays. Acta Neuropathol. *125*, 913–916.

Huth, L., Rose, M., Kloubert, V., Winkens, W., Schlensog, M., Hartmann, A., Knuchel, R., and Dahl, E. (2014). BDNF is associated with SFRP1 expression in luminal and basal-like breast cancer cell lines and primary breast cancer tissues: a novel role in tumor suppression? PLoS One *9*, e102558.

Jagani, Z., Mora-Blanco, E.L., Sansam, C.G., McKenna, E.S., Wilson, B., Chen, D., Klekota, J., Tamayo, P., Nguyen, P.T., Tolstorukov, M., et al. (2010). Loss of the tumor suppressor Snf5 leads to aberrant activation of the Hedgehog-Gli pathway. Nat. Med. *16*, 1429–1433.

Jones, D.T., Jäger, N., Kool, M., Zichner, T., Hutter, B., Sultan, M., Cho, Y.J., Pugh, T.J., Hovestadt, V., Stutz, A.M., et al. (2012). Dissecting the genomic complexity underlying medulloblastoma. Nature *488*, 100–105.

Kool, M., Jones, D.T., Jager, N., Northcott, P.A., Pugh, T.J., Hovestadt, V., Piro, R.M., Esparza, L.A., Markant, S.L., Remke, M., et al. (2014). Genome sequencing of SHH medulloblastoma predicts genotype-related response to smoothened inhibition. Cancer Cell *25*, 393–405.

Kung, A.L., Rebel, V.I., Bronson, R.T., Ch'ng, L.E., Sieff, C.A., Livingston, D.M., and Yao, T.P. (2000). Gene dose-dependent control of hematopoiesis and hematologic tumor suppression by CBP. Genes Dev. *14*, 272–277.

Lawrence, M., Huber, W., Pages, H., Aboyoun, P., Carlson, M., Gentleman, R., Morgan, M.T., and Carey, V.J. (2013). Software for computing and annotating genomic ranges. PLoS Comput. Biol. *9*, e1003118.

Li, Z., Tan, F., and Thiele, C.J. (2007). Inactivation of glycogen synthase kinase-3beta contributes to brain-derived neutrophic factor/TrkB-induced resistance to chemotherapy in neuroblastoma cells. Mol. Cancer Ther. *6*, 3113–3121.

Lin, C.Y., Erkek, S., Tong, Y., Yin, L., Federation, A.J., Zapatka, M., Haldipur, P., Kawauchi, D., Risch, T., Warnatz, H.J., et al. (2016). Active medulloblastoma enhancers reveal subgroup-specific cellular origins. Nature *530*, 57–62.

Liu, X., Wang, L., Zhao, K., Thompson, P.R., Hwang, Y., Marmorstein, R., and Cole, P.A. (2008). The structural basis of protein acetylation by the p300/CBP transcriptional coactivator. Nature *451*, 846–850.

Love, M.I., Huber, W., and Anders, S. (2014). Moderated estimation of fold change and dispersion for RNA-seq data with DESeq2. Genome Biol. *15*, 550.

Machold, R., and Fishell, G. (2005). Math1 is expressed in temporally discrete pools of cerebellar rhombic-lip neural progenitors. Neuron *48*, 17–24.

Mao, J., Ligon, K.L., Rakhlin, E.Y., Thayer, S.P., Bronson, R.T., Rowitch, D., and McMahon, A.P. (2006). A novel somatic mouse model to survey tumorigenic potential applied to the Hedgehog pathway. Cancer Res. *66*, 10171–10178.

Marino, S., Hoogervoorst, D., Brandner, S., and Berns, A. (2003). Rb and p107 are required for normal cerebellar development and granule cell survival but not for Purkinje cell persistence. Development *130*, 3359–3368.

Matei, V., Pauley, S., Kaing, S., Rowitch, D., Beisel, K.W., Morris, K., Feng, F., Jones, K., Lee, J., and Fritzsch, B. (2005). Smaller inner ear sensory epithelia in Neurog 1 null mice are related to earlier hair cell cycle exit. Dev. Dyn. *234*, 633–650.

Miller, R.W., and Rubinstein, J.H. (1995). Tumors in Rubinstein-Taybi syndrome. Am. J. Med. Genet. *56*, 112–115.

Mullighan, C.G., Zhang, J., Kasper, L.H., Lerach, S., Payne-Turner, D., Phillips, L.A., Heatley, S.L., Holmfeldt, L., Collins-Underwood, J.R., Ma, J., et al. (2011). CREBBP mutations in relapsed acute lymphoblastic leukaemia. Nature *471*, 235–239.

Ng, P.C., and Henikoff, S. (2003). SIFT: predicting amino acid changes that affect protein function. Nucleic Acids Res. *31*, 3812–3814.

Northcott, P.A., Buchhalter, I., Morrissy, A.S., Hovestadt, V., Weischenfeldt, J., Ehrenberger, T., Grobner, S., Segura-Wang, M., Zichner, T., Rudneva, V.A., et al. (2017). The whole-genome landscape of medulloblastoma subtypes. Nature *547*, 311–317.

Ohli, J., Neumann, J.E., Grammel, D., and Schuller, U. (2015). Localization of SHH medulloblastoma in mice depends on the age at its initiation. Acta Neuropathol. *130*, 307–309.

Oike, Y., Hata, A., Mamiya, T., Kaname, T., Noda, Y., Suzuki, M., Yasue, H., Nabeshima, T., Araki, K., and Yamamura, K. (1999). Truncated CBP protein leads to classical Rubinstein-Taybi syndrome phenotypes in mice: implications for a dominant-negative mechanism. Hum. Mol. Genet. *8*, 387–396.

Oliver, T.G., Grasfeder, L.L., Carroll, A.L., Kaiser, C., Gillingham, C.L., Lin, S.M., Wickramasinghe, R., Scott, M.P., and Wechsler, R. (2003). Transcriptional profiling of the Sonic hedgehog response: a critical role for N-myc in proliferation of neuronal precursors. Proc. Natl. Acad. Sci. USA *100*, 7331–7336.

Olson, M.V., Johnson, D.G., Jiang, H., Xu, J., Alonso, M.M., Aldape, K.D., Fuller, G.N., Bekele, B.N., Yung, W.K., Gomez-Manzano, C., et al. (2007). Transgenic E2F1 expression in the mouse brain induces a human-like bimodal pattern of tumors. Cancer Res. *67*, 4005–4009.

Pasqualucci, L., Dominguez-Sola, D., Chiarenza, A., Fabbri, G., Grunn, A., Trifonov, V., Kasper, L.H., Lerach, S., Tang, H., Ma, J., et al. (2011). Inactivating mutations of acetyltransferase genes in B-cell lymphoma. Nature *471*, 189–195.

Peifer, M., Fernandez-Cuesta, L., Sos, M.L., George, J., Seidel, D., Kasper, L.H., Plenker, D., Leenders, F., Sun, R., Zander, T., et al. (2012). Integrative genome analyses identify key somatic driver mutations of small-cell lung cancer. Nat. Genet. *44*, 1104–1110.

Petrij, F., Giles, R.H., Dauwerse, H.G., Saris, J.J., Hennekam, R.C., Masuno, M., Tommerup, N., van Ommen, G.J., Goodman, R.H., Peters, D.J., et al. (1995). Rubinstein-Taybi syndrome caused by mutations in the transcriptional co-activator CBP. Nature *376*, 348–351.

Puehringer, D., Orel, N., Luningschror, P., Subramanian, N., Herrmann, T., Chao, M.V., and Sendtner, M. (2013). EGF transactivation of Trk receptors regulates the migration of newborn cortical neurons. Nat. Neurosci. *16*, 407–415.

Rauskolb, S., Zagrebelsky, M., Dreznjak, A., Deogracias, R., Matsumoto, T., Wiese, S., Erne, B., Sendtner, M., Schaeren-Wiemers, N., Korte, M., et al. (2010). Global deprivation of brain-derived neurotrophic factor in the CNS reveals an area-specific requirement for dendritic growth. J. Neurosci. *30*, 1739–1749.

Robinson, G., Parker, M., Kranenburg, T.A., Lu, C., Chen, X., Ding, L., Phoenix, T.N., Hedlund, E., Wei, L., Zhu, X., et al. (2012). Novel mutations target distinct subgroups of medulloblastoma. Nature *488*, 43–48.

Schüller, U., Heine, V.M., Mao, J., Kho, A.T., Dillon, A.K., Han, Y.G., Huillard, E., Sun, T., Ligon, A.H., Qian, Y., et al. (2008). Acquisition of granule neuron precursor identity is a critical determinant of progenitor cell competence to form Shh-induced medulloblastoma. Cancer Cell *14*, 123–134.

Schwartz, P.M., Borghesani, P.R., Levy, R.L., Pomeroy, S.L., and Segal, R.A. (1997). Abnormal cerebellar development and foliation in BDNF–/– mice reveals a role for neurotrophins in CNS patterning. Neuron *19*, 269–281.

Smoll, N.R. (2012). Relative survival of childhood and adult medulloblastomas and primitive neuroectodermal tumors (PNETs). Cancer *118*, 1313–1322.

Soriano, P. (1999). Generalized lacZ expression with the ROSA26 Cre reporter strain. Nat. Genet. *21*, 70–71.

Sudarov, A., and Joyner, A.L. (2007). Cerebellum morphogenesis: the foliation pattern is orchestrated by multi-cellular anchoring centers. Neural Dev. *2*, 26.

Tanaka, Y., Naruse, I., Maekawa, T., Masuya, H., Shiroishi, T., and Ishii, S. (1997). Abnormal skeletal patterning in embryos lacking a single Cbp allele: a partial similarity with Rubinstein-Taybi syndrome. Proc. Natl. Acad. Sci. USA *94*, 10215–10220.

Taylor, M.D., Mainprize, T.G., Rutka, J.T., Becker, L., Bayani, J., and Drake, J.M. (2001). Medulloblastoma in a child with Rubenstein-Taybi syndrome: case report and review of the literature. Pediatr. Neurosurg. *35*, 235–238.

Taylor, M.D., Northcott, P.A., Korshunov, A., Remke, M., Cho, Y.J., Clifford, S.C., Eberhart, C.G., Parsons, D.W., Rutkowski, S., Gajjar, A., et al. (2012). Molecular subgroups of medulloblastoma: the current consensus. Acta Neuropathol. *123*, 465–472.

Wang, V.Y., Rose, M.F., and Zoghbi, H.Y. (2005). Math1 expression redefines the rhombic lip derivatives and reveals novel lineages within the brainstem and cerebellum. Neuron *48*, 31–43.

Wefers, A.K., Warmuth-Metz, M., Poschl, J., von Bueren, A.O., Monoranu, C.M., Seelos, K., Peraud, A., Tonn, J.C., Koch, A., Pietsch, T., et al. (2014). Subgroup-specific localization of human medulloblastoma based on pre-operative MRI. Acta Neuropathol. *127*, 931–933.

Wu, X., Northcott, P.A., Dubuc, A., Dupuy, A.J., Shih, D.J., Witt, H., Croul, S., Bouffet, E., Fults, D.W., Eberhart, C.G., et al. (2012). Clonal selection drives genetic divergence of metastatic medulloblastoma. Nature *482*, 529–533.

Zhang, X., Odom, D.T., Koo, S.H., Conkright, M.D., Canettieri, G., Best, J., Chen, H., Jenner, R., Herbolsheimer, E., Jacobsen, E., et al. (2005). Genome-wide analysis of cAMP-response element binding protein occupancy, phosphorylation, and target gene activation in human tissues. Proc. Natl. Acad. Sci. USA *102*, 4459–4464.

Zhang, Z., Hofmann, C., Casanova, E., Schutz, G., and Lutz, B. (2004). Generation of a conditional allele of the CBP gene in mouse. Genesis *40*, 82–89.

Zhou, P., Porcionatto, M., Pilapil, M., Chen, Y., Choi, Y., Tolias, K.F., Bikoff, J.B., Hong, E.J., Greenberg, M.E., and Segal, R.A. (2007). Polarized signaling endosomes coordinate BDNF-induced chemotaxis of cerebellar precursors. Neuron *55*, 53–68.

Zhu, X., Li, Q., Chang, R., Yang, D., Song, Z., Guo, Q., and Huang, C. (2014). Curcumin alleviates neuropathic pain by inhibiting p300/CBP histone acetyltransferase activity-regulated expression of BDNF and cox-2 in a rat model. PLoS One *9*, e91303.

Zhuo, L., Theis, M., Alvarez-Maya, I., Brenner, M., Willecke, K., and Messing, A. (2001). hGFAP-cre transgenic mice for manipulation of glial and neuronal function in vivo. Genesis *31*, 85–94.

STAR★METHODS

KEY RESOURCES TABLE

REAGENT or RESOURCE	SOURCE	IDENTIFIER
Antibodies		
Rabbit polyclonal anti GFP	Santa Cruz Biotechnology	Cat # sc-8334, RRID:AB_641123
Mouse monoclonal anti FLAG	Sigma-Aldrich	Cat# F1804, RRID:AB_439685
Mouse monoclonal anti Histone H3	Active Motif	Cat# 39763, RRID:AB_11142498
Rabbit polyclonal anti Histone H3	Abcam	Cat# ab47915, RRID:AB_873860
Mouse monoclonal anti Ki67	Dako	Cat# M7249, RRID:AB_2250503
Rabbit polyclonal anti phospho Histone H3 (Ser10)	Cell Signaling Technology	Cat# 9701, RRID:AB_331535
Mouse monoclonal anti BrdU (MoBU-1)	Thermo Fisher Scientific	Cat# B35128, RRID:AB_2536432
Rabbit monoclonal anti cleaved Caspase-3 (Asp175)	Cell Signaling Technology	Cat# 9664, RRID:AB_2070042
Mouse monoclonal anti Pax6	Developmental Study Hybridoma Bank	RRID:AB_528427
Rabbit polyclonal anti GFAP	Dako	Cat# Z0334, RRID:AB_10013382
Rabbit polyclonal anti S100	Dako	Cat# Z0311, RRID:AB_10013383
Rabbit polyclonal anti Calbindin D-28K	Millipore	Cat# AB1778, RRID:AB_2068336
Rabbit polyclonal anti CREBBP	LifeSpan BioSciences	Cat# LS-B3360, RRID:AB_2083956
Mouse monoclonal anti BDNF	Abcam	Cat# ab203573, RRID:AB_2631315
Rabbit polyclonal anti BDNF	(Aguado et al., 2007)	N/A
Rabbit polyclonal anti GLI1 (V812)	Cell Signaling Technology	Cat# 2534, RRID:AB_2294745
Goat polyclonal anti GLI3	R&D Systems	Cat# AF3690, RRID:AB_2232499
Mouse monoclonal anti β-Tubulin (TUB 2.1)	Sigma-Aldrich	Cat# T4026, RRID:AB_477577
Chicken polyclonal anti Calreticulin	Thermo Fisher Scientific	Cat# PA1-902A, RRID:AB_2069607
Bacterial and Virus Strains		
pIRES-GFP	This paper	N/A
pCre-IRES-GFP	This paper	N/A
Biological Samples		
Human medulloblastoma tissue samples	This paper	N/A
Chemicals, Peptides, and Recombinant Proteins		
BDNF recombinant human protein	Thermo Fisher Scientific	Cat# 10908010
ANA-12	Sigma-Aldrich	Cat# SML0209, CAS: 219766-25-3
Cyclotraxin-B (CTB)	Tocris	Cat# 5062, CAS: 1203586-72-4
N-2 Supplement	Gibco	Cat# 15410294, CAS: 10102-18-8
B27 Supplement	Thermo Fisher Scientific	Cat# 17504044
bFGF recombinant human protein	Thermo Fisher Scientific	Cat# 13256029, CAS: 106096-93-9
Mouse EGF	Sigma-Aldrich	Cat# SRP3196
Critical Commercial Assays		
Click-iT EdU Alexa Fluor 488 Imaging Kit	Thermo Fisher Scientific	Cat# C10337
Anti-FLAG M2 Affinity Gel	Sigma-Aldrich	Cat# A2220
EpiSeeker ChIP Kit – Histone H3 (acetyl)	Abcam	Cat# ab117150
SensiFAST™ SYBR® No-ROX Kit	Bioline	Cat# BIO-98005
EnVision+ System-HRP	Dako	Cat# K4007
High Capacity cDNA Reverse Transcription Kit	Thermo Fisher Scientific	Cat# 4368814
Deposited Data		
Microarray Super Series Raw and analyzed data	This paper	GEO: GSE107263
Experimental Models: Cell Lines		
Human embryonic kidney cells: HEK293T	ATCC	Cat# CRL-3216

(*Continued on next page*)

Continued

REAGENT or RESOURCE	SOURCE	IDENTIFIER
Experimental Models: Organisms/Strains		
Mouse: SmoM2^{loxP}	Jackson Laboratory	JAX# 005130
Mouse: Math1-Cre	Jackson Laboratory	JAX# 011104
Mouse: Math1-CreER^{T2}	Jackson Laboratory	JAX# 007684
Mouse: hGFAP-Cre	Jackson Laboratory	JAX# 004600
Mouse: Crebbp^{loxP}	(Zhang et al., 2004)	N/A
Mouse: Bdnf^{loxP}	(Rauskolb et al., 2010)	N/A
Oligonucleotides		
Forward primer for Beta-2 microglobulin, CCTGGTCTTTCTGGTGCTTG	This paper	N/A
Reverse primer for Beta-2 microglobulin, TATGTTCGGCTTCCCATTCT	This paper	N/A
Forward primer for Crebbp, AGTCATCACAGCAGCAACCA	This paper	N/A
Reverse primer for Crebbp, GCACCTCTGTCTTCATTTCCA	This paper	N/A
Forward primer for Bdnf, ACAAGGCAACTTGGCCTACC	This paper	N/A
Reverse primer for Bdnf, TCGTCAGACCTCTCGAACCT	This paper	N/A
Forward primer for Bdnf promoter P1, TCATCACTCACGACCACGTC	This paper	N/A
Reverse primer for Bdnf promoter P1, GCCTCTCTGAGCCAGTTACG	This paper	N/A
Forward primer for Bdnf promoter P4, GCGCGGAATTCTGATTCTGG	This paper	N/A
Reverse primer for Bdnf promoter P4, AAAGTGGGTGGGAGTCCA	This paper	N/A
Recombinant DNA		
Plasmid: pBabe-puro-FLAG-hCREBBP-IRES-GFP	This paper	N/A
Plasmid: pBabe-puro-FLAG-hCREBBP-R1446L-IRES-GFP	This paper	N/A
Plasmid: pBabe-puro-FLAG-hCREBBP-Y1482C-IRES-GFP	This paper	N/A
Plasmid: pBabe-puro-FLAG-hCREBBP-I1483F-IRES-GFP	This paper	N/A
Software and Algorithms		
FIJI	NIH	https://imagej.net/Fiji/Downloads
PyMOL	Schrodinger	https://pymol.org/2/
Cytoscape	National Institute of General Medical Sciences	http://www.cytoscape.org/download.php
GSEA	Broad Institute	http://software.broadinstitute.org/gsea/index.jsp
R: A Language and Environment for Statistical Computing	R Core Team	https://www.R-project.org

CONTACT FOR REAGENT AND RESOURCE SHARING

Further information and requests for resources and reagents should be directed and will be fulfilled by the Lead Contact, Ulrich Schüller (u.schueller@uke.de).

EXPERIMENTAL MODEL AND SUBJECT DETAILS

Mice

SmoM2-YFP$^{Fl/Fl}$ (Mao et al., 2006), *hGFAPCre* (Zhuo et al., 2001), *Math1CreER*^{T2} (Machold and Fishell, 2005) and ROSA26lacZ$^{Fl/Fl}$ (Soriano, 1999) mice were obtained from The Jackson Laboratory (Bar Harbour, ME, USA). Generation of *Math1Cre*, *Crebbp*$^{Fl/Fl}$ and *Bdnf*$^{Fl/Fl}$ mice has previously been described (Rauskolb et al., 2010; Matei et al., 2005; Zhang et al., 2004). Genotyping was performed by PCR using DNA from tail genomic DNA. All mice were maintained on a 12 h dark/light cycle and housed with a maximum of five mice per cage. We used animals of both sexes for the experiments. All experimental procedures were approved by the Government of Upper Bavaria, Germany (Reference number 55.2-1-54-2532-10-14).

Cell Culture

HEK293T cells were cultivated in DMEM medium supplemented with 10% FCS, glutamine (2 mM) and Pen/Strep (100 μg/ml) at 37°C, 5% CO_2. HEK293T cells derive from a female donor. Cells were seeded at 1 million cells per 10 cm dish and typically reached confluency 48 h after seeding. For sub-culturing, cells were detached with Trypsin-EDTA (0.25%), washed once and seeded on a new dish.

Primary Cell Cultures

For all primary cultures, animals were decapitated under anesthesia and cerebella were dissected and freed of meninges and choroid plexus. For GNP cultures, cerebella from P5 mice were incubated in Trypsin/EDTA (0.25%) solution for 10 min and mechanically minced. GNPs were grown on poly-L-ornithine-coated wells in DMEM:F12 (Gibco) media containing 10% fetal calf serum (Gibco) for 6 h before changing to serum-free medium (DMEM:F12, N-2 supplement, 25 mM KCl and 100 μg/ml Pen/Strep) containing SHH (3 μg/ml) for 24 h prior to virus infection. For cerebellar explant cultures, cerebella from P3 mice were cut into small pieces which were passed through a 400 μm nylon mesh. Resulting cerebellar pieces were grown on poly-L-ornithine/laminin-coated coverslips for 5 days in DMEM:F12 media (Gibco) with N-2 supplement, 25mM KCl and 10% fetal calf serum. For rescue experiments, the medium was supplemented with human BDNF protein (200 ng/ml) and explants were maintained in culture for 5 days, changing the medium every 2 days. Tumor cell culture was performed as described for culturing GNPs with the following exceptions: tumor cells were maintained in Neurobasal media containing B27 supplement, human bFGF (20 ng/ml), mouse EGF (20 ng/ml), glutamine (2 mM) and Pen/Strep (100 μg/ml).

METHOD DETAILS

Mice Treatments

For analysis of proliferation *in vivo*, mice were pulse labelled with EdU (5-ethynyl-2-deoxyuridine; Sigma-Aldrich) and/or BrdU (5-bromo-2-deoxyuridine; Sigma-Aldrich) at a concentration of 20.53 μg/g or 25 μg/g body weight, respectively. For the induction of Cre activity in *Math1-creER*^{T2} mice, pregnant dams or pubs were injected with 1 mg tamoxifen dissolved in corn oil intraperitoneally.

Orthotopic Transplantation of Tumor Cells

Tumor cells from *Math1-cre::Crebbp*$^{Fl/+}$*SmoM2-YFP*$^{Fl/+}$ and *Math1-cre::Crebbp*$^{Fl/Fl}$*SmoM2-YFP*$^{Fl/+}$ mice were isolated when tumor-prone mice showed clinical symptoms. Mice were killed by cervical dislocation, the skull was opened under sterile conditions and the tumor was dissected in HBSS solution (supplemented with 6 g/l glucose, pH 7.4). Tumor was washed once in HBSS solution and incubated in Trypsin-EDTA (Sigma-Aldrich; supplemented with DNAse 100 μg/ml) at 37°C for 10 min. Next, trypsin was inactivated by adding culture medium supplemented with 10 % fetal calf serum and tumors were subsequently isolated by pipetting up and down. Finally, cells were counted in a Neubauer chamber and 600.000 cells were transplanted into cerebella of wild type mice. For allogenic transplantation of tumor cells, recipient mice were orally treated with Novalgin (25 μg per g body weight) 30 min before transplantation. For anesthesia, mice were injected with "Hellabrunner solution" (1.1 mg/ml xylazine, 12.8 mg/ml ketamine, 1.2 mg/ml acepromazine in 0.9 % NaCl solution) intraperitoneally. Mice were stereotactically fixed, a small incision was made to be able to see Lamda coordinates on the skull. A small hole was drilled in the midline 3 mm caudal from Lamda. Cell suspensions were injected using a 20 gauge needle over a period of 2 minutes, after which the needle was left in place for additional 2 minutes before being retracted with caution. Wounds were sutured and wound areas were disinfected properly. After the manipulation, animals were monitored one every hour for a duration of 6 hours. During the process of tumor formation, animals were monitored once a day for tumor-associated symptoms such as ataxia und lethargy.

Pulse Labeling GNP Cultures

After incubation with viral supernatant, cells were maintained in SHH-supplemented medium for the indicated period of time. To determine proliferative activity, cells were pulsed with BrdU 2 h prior to fixation in 4 % paraformaldehyde. For cell cycle analysis, transduced cells were initially labelled with EdU for 2h, further cultured and secondarily labeled with BrdU after indicated incubation periods to determine the fraction of double labelled cells in the transduced cell population.

Production of Retroviral Particles

For production of retroviral particles, HEK293T cells were co-transfected using X-tremeGene (Roche) with retroviral constructs encoding for either *IRES-GFP* or *Cre-IRES-GFP* sequences together with plasmids encoding for *gag-pol* and *Vsv-g* constructs. Packaging cells were re-fed 12 h after transfection and retroviral supernatants were collected every 24 h for three days. Supernatants were pooled and stored at -80°C.

Generation of FLAG-Tagged CREBBP Mutants

A mammalian expression vector encoding the human CREBBP protein with an N-terminal FLAG tag was used in this study (pBabe-puro-FLAG-CREBBP-IRES-GFP). A site-directed mutagenesis protocol based on an assembly PCR reaction was used to create intragenic *AgeI*/*MluI*-fragments of human *CREBBP* carrying the desired mutation (primer sequences available upon request). The presence of the desired mutations and the integrity of the open reading frame were confirmed in all constructs by enzymatic digestion and sequencing.

Isolation of Recombinant FLAG-Tagged Proteins

HEK 293T cells were used for the expression of FLAG-tagged CREBBP proteins. FLAG-tagged proteins were isolated using the FLAG Immunoprecipitation Kit (Sigma-Aldrich). Purity and integrity of isolated FLAG-tagged proteins was assessed by western blot. For assessment of protein concentration, extinction coefficients and molecular weight for all FLAG-tagged CREBBP forms were calculated using the ProtParam tool (www.expasy.org). Finally, absorbance at 280 nm was measured (NanoDrop) and protein concentrations were calculated according to Beer's law.

Protein Structures and *In Vitro* Acetylation Assay

The crystal structure of the EP300 HAT domain was previously deposited at RCSB PDB (www.pdb.org) under accession code 3BIY. Acetyltransferase (HAT) activity was assessed using the Histone Acetyltransferase Activity Assay Kit (Abcam) according to manufacturer's instructions. Briefly, 200 ng of purified human CREBBP protein (wild-type or selected mutants) were subjected to the *in vitro* acetylation assay in a 96 well plate. The plate was incubated at 37°C in an absorbance reader (Optima) and absorbance at 450 nm was measured every hour for a period of 5 hours. For data analysis, background absorbance of a negative control was subtracted from each sample at the respective time point. HAT activity is expressed as relative absorbance value per μg protein.

Generation of Stable HEK293T CREBBP Clones

HEK293T cells were cultivated in DMEM medium supplemented with 10% FCS, glutamine (2 mM) and Pen/Strep (100 μg/ml). Cells were transfected with pBabe-puro-FLAG-IRES-GFP constructs carrying respective human SHH-MB associated CREBBP mutants using the calcium phosphate method and subsequently selected with 2 μg/ml puromycin to generate monoclonal, single-cell populations.

Analysis of Histone Acetylation

Stably transfected HEK293T clones were seeded on slides, fixed in formaldehyde the following morning for 1h at room temperature and blocked in 10% normal goat serum in PBS for 30 min. Cells were incubated with primary antibodies against histone H3, acetyl histone H3 and GFP for 1h at room temperature. Subsequently, cells were washed 3 times and incubated with secondary antibodies (goat anti mouse Alexa555, ab150114, Abcam; goat anti rabbit Alexa488, A-11034, Life Technologies; goat anti rat Alexa647, ab150159, Abcam) for 1h at room temperature, washed and counterstained with DAPI. Images were acquired and individual nuclei with clear GFP signal were masked on the basis of the DAPI signal. Analysis of images was performed using ImageJ. For each image, the mean background signal was determined using least 5 different areas free of any cell bodies. Next, the integrated densities and the area were measured for each GFP-positive nucleus. The corrected total cell fluorescence (CTCF) for histone H3 and acetyl histone H3 for each nucleus was determined as follows:

$$\text{CTCF} = \text{Integrated Density} - (\text{Area} * \text{Mean Background signal})$$

Immunohistochemistry and Image Quantification

Immunohistochemistry on paraffin-embedded sections was performed using standard protocols with primary antibodies under optimized conditions. Visualization was performed using EnVision + System-HRP/DAB (DAKO) according to manufacturer's recommendations. Sections developed with the EnVision + System were counterstained with hematoxylin to stain cell nuclei. To visualize EdU in combination with BrdU, we applied the Click-iT EdU Imaging Kit (Thermo Fisher) in combination with MoBu-1 BrdU antibody. EdU/BrdU double stainings were visualized with secondary antibodies coupled with Alexa 488/555 fluorophores and counterstained with Hoechst33342. For all quantifications of cellular markers in the EGL, we used pictures from lobules IV and V of the cerebellum for better comparison. To determine the fraction of cells in the EGL positive for a specific marker, we counted the total number of cells in the EGL (identified by Hematoxylin stain) and the number of cells positive for the marker (chromogenic signal or fluorescent signal for double stainings). ImageJ was used for counting.

X-gal Stainings

For detection of β-galactosidase in cryosections, unfixed material was equilibrated in PBS, incubated in X-gal working solution (2 mg/ml X-gal, 5 mM $K_4Fe(CN)_6$, 5 mM $K_3Fe(CN)_6$, 2 mM $MgCl_2$, 0.02% NP40 and 0.1% sodium deoxycholate in PBS) for 3 h, washed n PBS and counterstained in Kernechtrot.

Immunocytochemistry

Immunohistochemistry of all cell cultures was carried out by fixing the cells for 30 min in formaldehyde and blocking the cells in 10% normal goat serum. Subsequently, cells were incubated with primary antibodies. Primary antibodies can be seen in the Key Resources Table. Secondary antibodies were goat anti mouse Alexa488 (A-11-29, Life Technologies), goat anti rabbit Alexa555 (ab150078, Abcam) or goat anti rat Alexa 647 (ab150159, Abcam). Cultures were counterstained with DAPI.

Western Blot Analysis

Protein was extracted using RIPA buffer, separated electrophoretically in NuPAGE 4 – 20 % Bis-Tris or 3 – 8 % Tris-Acetate gels (Thermofisher) and blotted on a PVDF membrane (Millipore) using standard procedures. Optimal concentrations for all antibodies were evaluated empirically. Protein bands were visualized using horse radish peroxidase (HRP)-coupled secondary antibodies (BioRad) and SuperSignal West Dura solution as substrate (Thermofisher). Image acquisition was done using either ImageQuant LAS 4000 (GE Healthcare Life Sciences) or HyBlot CL autoradiography film (Denville Scientific). For western blot analyses of BDNF protein, 40 μg of protein extract were diluted to a total volume of 20μl with Laemmli buffer and incubated at 99°C for 5 minutes. Samples were then centrifuged at 13.400rpm for 90s, using an Eppendorf Mini Spin centrifuge before loading on 18% PAA gels. After electrophoresis, proteins were blotted on Immuno-Blot PVDF membranes (Roth, BioRad) using a BioRad Trans Blot Semi Dry (SD) chamber. Blocking and antibody incubation was performed in heat-inactivated and filtered 1xTBST, 10% goat-serum, 5% milkpowder (Biorad) for 3–4h. For BDNF detection, rabbit anti-BDNF (Aguado et al., 2007) was used at 1:4000 in blocking solution and incubated at 4°C overnight. Chicken anti Calreticulin in 1xTBST, 0,01% NaN_3 as a loading control. For detection, ECL Plus-kit (GE-Healthcare) was used in combination with horseradish peroxidase-coupled secondary antibodies (Jackson Immuno-research).

Quantitative Real Time PCR (qRT-PCR)

RNA from mouse tumors was extracted using Trizol (Invitrogen) according to manufacturer's protocol. Reverse transcription was performed using the High Capacity cDNA Reverse Transcription Kit (Applied Biosystems) according to manufacturer's specifications. For Crebbp, Bdnf and β2m, PCR reactions were performed in triplicates using the SensiFAST SYBR No-ROX Kit (Bioline) in a LightCycler480 Instrument (Roche). For each set of primers, postamplification melting curves were analyzed using the LightCycler480 software to ensure selective amplification of the desired product. The housekeeper gene *Beta-2*-micoglobulin was used in qRT-PCR for relative quantification. qRT-PCR for Gli1, Gli2, Gli3, Ptch1, Smo and Sufu was performed using Taqman gene expression assays with the following Taqman probes: *Gli1* Mm00494645_m1, *Gli2* Mm01293117_m1, *Gli3* Mm00492333_m1, *Ptch1* Mm00970977_m1, *Smo* Mm01162710_m1, and *Sufu* Mm00489385_m1. Values were normalized to *Gapdh* levels.

Chromatin Immunoprecipitations

ForChIP-qPCR, the EpiSeeker ChIP Kit – Histone H3 (acetyl) – Tissue Kit (abcam) was used according to manufacturer's recommendations. Quantification of immunoprecipitated DNA was performed using qRT-PCR with primers specific for Bdnf promoters P1 and P4. Each ChIP DNA fraction was normalized to the corresponding Input DNA fraction to account for chromatin sample preparation differences. Normalized ChIP fractions for replicate samples were averaged. Mock immunoprecipitations using a mouse IgG antibody were included as a control. Finally, percent of input DNA values for each ChIP fraction were calculated by linear conversion.

Microarray and Gene Ontology Analysis

Total RNA was extracted from whole cerebella. For global gene expression profiles, hybridization was performed on GeneChip Mouse Gene 2.0 ST Arrays (Affymetrix) and normalized using the Robust Multi-Array Average method. An empirical Bayes moderated t-statistics approach implemented in the LIMMA package for R was used for differential expression detection. The Benjamini and Hochberg's approach was used to control for false discoveries. Cluster analyses were performed using Morpheus (Broad Institute) or TM4 Microarray Software Suite (MeV v4.8) using Pearson correlation with average linkage. Gene Ontology analysis was performed using the Compact Compare of Annotations tool from g:Profiler (http://biit.cs.ut.ee/gprofiler/) using the list of differentially expressed genes. As reference, data from the Gene Ontology Consortium, the KEGG pathway and the Reactome database were used. Summarization of GO terms in enrichment maps was performed using REVIGO (http://revigo.irb.hr/) and visualized using Cytoscape.

Sequencing of Human Tumor Samples

For tumors from the Munich cohort, the *CREBBP* gene (NM_004380) was amplified by PCR using AmpliTaq Gold and AccuPrime Polymerase Systems (Life Technologies, Carlsbad) with optimized primers (primer sequences will be made available upon request). PCR products were subjected to Sanger sequencing using the Big Dye Terminator v1.1 Cycle Sequencing Kit (Life Technologies).

Sequence analysis was performed using an ABI PRISM 3130 Genetic Analyzer. The identified alterations were compared to the dbSNP database (build 144) and the Exome Variant Server, NHLBI Exome Sequencing Project (ESP) (data release ESP6500SI-V0.3.1) to identify known single nucleotide polymorphisms.

RNA-Seq and Differential Gene Expression Analysis

For tumors from the Heidelberg cohort, RNA-seq data was collected (MB53, MB56, MB59, MB60, MB61, MB63) from a previous study (Northcott et al., 2017). All reads were aligned to human reference genome hs37d5 using STAR (Dobin et al., 2013) (version STAR_2.3.0e_r291), with parameters ''–outSAMunmapped within –outQSconversionAdd 0 –outFilterMultimapNmax 1''. Raw read counts were calculated using the R/Bioconductor package GenomicAlignments (Lawrence et al., 2013) and gene annotation from Gencode 19 (https://www.gencodegenes.org/releases/19.html). For tumors from the Toronto cohort, sequence reads were aligned using STAR (v.2.5.1b) against hg19, with quantMode enabled for GeneCounts, and gene annotations derived from Gencode 19. Differential gene expression analysis was performed using the R/Bioconductor package DESeq2 (Love et al., 2014).

Gene Set Enrichment Analysis (GSEA)

GSEA for gene expression data was performed using the indicated gene set collections from the Molecular Signature Database (Broad Institute) using 1000 gene set permutations and a FDR threshold of 5% according to recommendations by the Broad Institute. For GSEA on expression data derived from RNA-seq analyses, we used the GSEAPreranked tool (Broad Institute). In here, genes were ranked based on their log2 fold change between CREBBP wild type and mutation groups as determined by DESeq2.

Publication Consent for Human Data

Written informed consent was provided for the publication of all shown magnetic resonance images.

QUANTIFICATION AND STATISTICAL ANALYSIS

All data presented are mean ± s.e.m., and each data point represents an individual animal or experiment. Graphs illustrating experiments with $n < 5$ show individual data points. Statistical analyses were done using the Prism4 software (Graph Pad). P values < 0.05 were considered significant ($^{*}P < 0.05$, $^{**}P < 0.01$, $^{***}P < 0.001$, $^{****}P < 0.0001$). The unpaired t test (two-tailed) or paired t test (two-tailed) was applied to compare the means of two groups. For comparison of three or more groups, the ordinary one-way ANOVA with *post-hoc* Bonferroni test for multiple comparisons was applied. Time course experiments with three or more groups were analyzed using the two-way repeated measures ANOVA with *post-hoc* Bonferroni test for multiple comparisons. For comparison of categorical variables in a contingency table, the Fisher's exact test was used. Kaplan-Meier survival curves were established to analyze the survival of mice and patients, respectively. The log-rank test was used to examine the significance of results. For correlation analyses of gene expression across different samples, we used a Pearson correlation approach.

DATA AND SOFTWARE AVAILABILITY

The complete gene expression values are accessible as part of previously reported series through GEO Series accession numbers GEO: GSE49243, GSE10327, and GSE37418. Accession numbers and corresponding databases for sequencing data can be retrieved from Kool et al., (2014). Data from the Toronto cohort have been deposited at the European Genome-phenome Archive under accession number EGAD00001001461. All microarray generated in this study and herein published for the first time have been deposited under the accession number GEO: GSE107263.